JNeurosci Accepted Manuscript

This Accepted Manuscript has not been copyedited and formatted. The final version may differ from this version.

JNeurosci
THE JOURNAL OF NEUROSCIENCE

Research Articles: Systems/Circuits

Tenuous inhibitory GABAergic signaling in the reticular thalamus

Peter M. Klein[1], Adam Lu[1], Megan E. Harper[1], Hannah M. McKown[1], Jessica Morgan[1] and Mark P. Beenhakker[1]

[1]*Department of Pharmacology, University of Virginia School of Medicine, Charlottesville, Virginia 22903*

DOI: 10.1523/JNEUROSCI.1345-17.2017

Received: 9 May 2017

Revised: 20 September 2017

Accepted: 3 November 2017

Published: 22 December 2017

Author contributions: P.M.K., A.L., and M.P.B. designed research; P.M.K., A.L., M.E.H., H.M.M., and J.D.M. performed research; P.M.K., A.L., M.E.H., H.M.M., and M.P.B. analyzed data; P.M.K., A.L., and M.P.B. wrote the paper.

Conflict of Interest: The authors declare no competing financial interests.

The authors thank Vivek Jayaraman, Ph.D., Douglas S. Kim, Ph.D., Loren L. Looger, Ph.D., Karel Svoboda, Ph.D. from the GENIE Project, Janelia Research Campus, HHMI for permission to use the GCaMP6s construct. We thank Drs. Tarek Deeb and Paul Davies for guidance regarding perforated patch recordings. Kathryn Salvati and Dr. Ruth Stornetta provided invaluable guidance for our anatomical experiments. This work was supported by NIH/NIGMS T32 training grant T32GM008328-24 and NIH Grant R01NS099586-01

Corresponding author: Mark P. Beenhakker, Department of Pharmacology, University of Virginia School of Medicine, 1340 Jefferson Park Avenue, Charlottesville, Virginia 22903. Email: MPB5Y@virginia.edu

Cite as: J. Neurosci ; 10.1523/JNEUROSCI.1345-17.2017

Alerts: Sign up at www.jneurosci.org/cgi/alerts to receive customized email alerts when the fully formatted version of this article is published.

Accepted manuscripts are peer-reviewed but have not been through the copyediting, formatting, or proofreading process.

Copyright © 2017 the authors

JNeurosci Accepted Manuscript

Title (50 word maximum): Tenuous inhibitory GABAergic signaling in the reticular thalamus

Abbreviated title (50 character maximum): GABAergic signaling in reticular thalamus

Author names and affiliation: Peter M. Klein,[1] Adam Lu,[1] Megan E. Harper,[1] Hannah M. McKown,[1] Jessica Morgan,[1] Mark P. Beenhakker[1]
[1]Department of Pharmacology, University of Virginia School of Medicine, Charlottesville, Virginia 22903

Corresponding author: Mark P. Beenhakker, Department of Pharmacology, University of Virginia School of Medicine, 1340 Jefferson Park Avenue, Charlottesville, Virginia 22903. Email: MPB5Y@virginia.edu

Number of pages: 47

Number of figures, tables, multimedia and 3D models (separately): 8

Number of words for Abstract, Introduction, and Discussion (separately):
Abstract – 233 (250 max)
Introduction – 567 (650 max)
Discussion – 1487 (1500 max)

Conflict of Interest: The authors declare no competing financial interests.

Acknowledgements: The authors thank Vivek Jayaraman, Ph.D., Douglas S. Kim, Ph.D., Loren L. Looger, Ph.D., Karel Svoboda, Ph.D. from the GENIE Project, Janelia Research Campus, HHMI for permission to use the GCaMP6s construct. We thank Drs. Tarek Deeb and Paul Davies for guidance regarding perforated patch recordings. Kathryn Salvati and Dr. Ruth Stornetta provided invaluable guidance for our anatomical experiments. This work was supported by NIH/NIGMS T32 training grant T32GM008328-24 and NIH Grant R01NS099586-01

JNeurosci Accepted Manuscript

1 **Abstract**

2 Maintenance of a low intracellular Cl^- concentration ($[Cl^-]_i$) is critical for enabling inhibitory 3 neuronal responses to $GABA_A$ receptor-mediated signaling. Cl^- transporters, including KCC2, 4 and extracellular impermeant anions ($[A]_o$) of the extracellular matrix are both proposed to be 5 important regulators of $[Cl^-]_i$. Neurons of the reticular thalamic (RT) nucleus express reduced 6 levels of KCC2, indicating that GABAergic signaling may produce excitation in RT neurons. 7 However, by performing perforated patch recordings and calcium imaging experiments in rats 8 (male and female), we find that $[Cl^-]_i$ remains relatively low in RT neurons. While we identify a 9 small contribution of $[A]_o$ to a low $[Cl^-]_i$ in RT neurons, our results also demonstrate that reduced 10 levels of KCC2 remain sufficient to maintain low levels of Cl^-. Reduced KCC2 levels, however, 11 restrict the capacity of RT neurons to rapidly extrude Cl^- following periods of elevated 12 GABAergic signaling. In a computational model of a local RT network featuring slow Cl^- 13 extrusion kinetics, similar to those we found experimentally, model RT neurons are predisposed 14 to an activity-dependent switch from GABA-mediated inhibition to excitation. By decreasing the 15 activity threshold required to produce excitatory GABAergic signaling, weaker stimuli are able to 16 propagate activity within the model RT nucleus. Our results indicate the importance of even 17 diminished levels of KCC2 in maintaining inhibitory signaling within the RT nucleus and suggest 18 how this important activity choke point may be easily overcome in disorders such as epilepsy.

19

20 **Significance Statement**

21 Precise regulation of intracellular Cl^- levels ($[Cl^-]_i$) preserves appropriate, often inhibitory, 22 GABAergic signaling within the brain. However, there is disagreement over the relative 23 contribution of various mechanisms that maintain low $[Cl^-]_i$. We found that the Cl^- transporter 24 KCC2 is an important Cl^- extruder in the reticular thalamic (RT) nucleus, despite this nucleus 25 having remarkably low KCC2 immunoreactivity relative to other regions of the adult brain. We 26 also identified a smaller contribution of fixed, impermeant anions ($[A]_o$) to lowering $[Cl^-]_i$ in RT

JNeurosci Accepted Manuscript

27 neurons. Inhibitory signaling among RT neurons is important for preventing excessive activation
28 of RT neurons, which can be responsible for generating seizures. Our work suggests that KCC2
29 critically restricts the spread of activity within the RT nucleus.
30

JNeurosci Accepted Manuscript

31 **Introduction**

32 Proper inhibitory neurotransmission in the central nervous system is critical for many neural
33 processes (Wong et al., 2003; Kaila et al., 2014) and is primarily mediated by the influx of
34 chloride (Cl^-) through the $GABA_A$ receptor. However, if the concentration of intracellular Cl^-
35 ($[Cl^-]_i$) is sufficiently elevated, then $GABA_A$ receptor activation enables Cl^- efflux and neuronal
36 depolarization (Cherubini et al., 1990; Rohrbough and Spitzer, 1996; Staley and Smith, 2001).
37 Thus, depending on the $[Cl^-]_i$, the actions of GABA can be either inhibitory or excitatory.

38 The low $[Cl^-]_i$ required for GABAergic inhibition is primarily achieved by active Cl^- extrusion
39 driven by the K^+-Cl^- cotransporter KCC2 (Payne et al., 1996; Rivera et al., 1999). However,
40 negatively charged, fixed macromolecules known as *impermeant anions* can also promote a low
41 $[Cl^-]_i$ (Donnan, 1911), perhaps even more prominently than KCC2 (Delpire and Staley, 2014;
42 Glykys et al., 2014a). To date, the relative contribution of KCC2 and impermeant anions to $[Cl^-]_i$
43 remains an open debate (Glykys et al., 2014b; Kaila et al., 2014; Luhmann et al., 2014; Voipio
44 et al., 2014; Doyon et al., 2016).

45 Evaluating the contributions of KCC2 and impermeant anions to GABAergic processes that
46 regulate global brain excitability is particularly pertinent for understanding seizure propagation.
47 The reticular thalamic (RT) nucleus envelops and critically regulates the nuclei of the dorsal
48 thalamus (Jones, 2007). Importantly, local circuitry within the RT nucleus operates as an
49 inhibitory choke point that prevents the propagation of seizures (Huntsman et al., 1999; Sohal
50 and Huguenard, 2003; Paz and Huguenard, 2015; Makinson et al., 2017). Notably, the RT
51 nucleus is one of the few adult brain regions with greatly reduced KCC2 expression (Kanaka et
52 al., 2001; Barthó et al., 2004; Sun et al., 2012). Indeed, the paucity of KCC2 in the RT nucleus
53 suggests that GABAergic neurotransmission within the nucleus is excitatory (Sun et al., 2012),
54 thus presenting a conundrum regarding the role of the RT nucleus as an inhibitory seizure
55 choke point.

JNeurosci Accepted Manuscript

56 Reciprocal GABAergic connections among RT neurons form the basis of the thalamic
57 seizure choke point (Ahlsén and Lindström, 1982; Yen et al., 1985; Pinault et al., 1997).
58 Eliminating these connections increases thalamic excitability (Huntsman et al., 1999; Makinson
59 et al., 2017) and possibly causes seizures (Homanics et al., 1997; DeLorey et al., 1998).
60 Computational modeling suggests that local GABAergic signaling among RT neurons prevents
61 the simultaneous activation of nearby neurons through an activity-vetoing mechanism, thereby
62 restricting seizure generation (Sohal and Huguenard, 2003). This model assumes that GABA is
63 inhibitory, an effect mediated by low $[Cl^-]_i$ (Ulrich and Huguenard, 1997). However, if GABA is
64 excitatory due to low KCC2 expression, it then remains unclear how the RT nucleus can
65 function as a seizure choke point.

66 In this study, we aim to better understand GABAergic regulation of excitability within the RT
67 nucleus. Using immunohistochemistry, we confirm a reduced KCC2 expression in the RT
68 nucleus and further demonstrate that it remains low throughout development. However, despite
69 low KCC2 immunoreactivity, intracellular, perforated patch clamp recordings of RT neurons
70 indicate that the $[Cl^-]_i$ is low, and that GABAergic signaling inhibits RT neurons. We then show
71 that impermeant anions, abundantly expressed in the RT nucleus, only moderately contribute to
72 a low RT $[Cl^-]_i$. Surprisingly, despite low RT immunoreactivity, KCC2 effectively regulates basal
73 $[Cl^-]_i$ in RT neurons. However, diminished KCC2 leaves RT neurons more susceptible to activity-
74 dependent Cl^- accumulation, likely weakening the capacity of the RT inhibitory choke point to
75 prevent seizures.

76

77 **Methods**

78 *Subjects.* Wild type Sprague-Dawley rats (Charles River Laboratories, Wilmington, MA) and wild
79 type C57Bl/6NJ mice (The Jackson Laboratory, Bar Harbor, ME) of either sex were utilized in
80 these experiments. All experiments were approved by the Institutional Care and Use Committee

JNeurosci Accepted Manuscript

81 at the University of Virginia (Charlottesville, VA), in accordance with the National Institutes of
82 Health guidelines.
83
84 *Intracerebroventricular injections.* In some instances, P0-2 rats received an
85 intracerebroventricular (ICV) injection of an AAV9.Syn.GCaMP6s.WPRE.SV40 viral vector
86 (Penn Vector Core, Philadelphia, PA, AV-1-PV2824; supplied by the GENIE Project, Janelia
87 Research Campus, HHMI) (Glascock et al., 2011). Sterile microliter calibrated glass pipettes
88 were filled with virus diluted to ~$1x10^{13}$ GC/ml in 0.1% trypan blue dye (Bio-Rad, Raleigh, NC).
89 Rats were cryoanesthetized and the pipette was lowered through the skull, into the lateral
90 ventricle. A picospritzer (Picospritzer III, Parker Hannifin, Hollis, NH) was used to deliver 3 µl of
91 virus solution into each lateral ventricle. Animals were then returned to the dam to allow time for
92 GCaMP6s expression.
93
94 *Slice preparation*. P10-20, animals were deeply anesthetized with pentobarbital and then
95 transcardially perfused with an ice-cold protective recovery solution containing (in mM): 92
96 NMDG, 26 $NaHCO_3$, 25 glucose, 20 HEPES, 10 $MgSO_4$, 5 Na-ascorbate, 3 Na-pyruvate, 2.5
97 KCl, 2 thiourea, 1.25 NaH_2PO_4, 0.5 $CaCl_2$, titrated to a pH of 7.3-7.4 with HCl (Ting et al., 2014).
98 Horizontal slices (250 µm) containing the thalamus were cut in ice-cold protective recovery
99 solution using a vibratome (VT1200, Leica Biosystems, Buffalo Grove, IL). Slices were trimmed
100 to remove the hippocampus and cortex, and then transferred to protective recovery solution
101 maintained at 32-34°C for 12 minutes. Brain slices were kept in room temperature aCSF
102 consisting of (in mM) 126 NaCl, 26 $NaHCO_3$, 10 glucose, 2.5 KCl, 2 $CaCl_2$, 1.25 NaH_2PO_4, 1
103 $MgSO_4$. All solutions were equilibrated with 95% O_2/5% CO_2.
104
105 *Electrophysiology*. Intracellular recordings were performed in a submerged chamber, with slices
106 situated on nylon netting and perfused with warm (31-33°C) oxygenated aCSF at 2.5 ml/min. All

JNeurosci Accepted Manuscript

107 experiments were performed in the presence of kynurenic acid (3 mM) and CGP 55845 (100
108 nM) to block AMPA, NMDA and $GABA_B$ receptors, and TTX (1 μM) to block sodium channel
109 activation. Cadmium chloride (100 μM) was used to block voltage-dependent calcium channel
110 activation in all Cl^- extrusion experiments. Thalamic neurons were visualized using infrared Dodt
111 gradient contrast illumination on a Zeiss Axio Examiner.A1 microscope (Zeiss Microscopy,
112 Thornwood, NY) and an sCMOS camera (ORCA-Flash4.0, Hamamatsu, Japan). Recording
113 pipettes were pulled from thick-walled borosilicate capillary glass (Sutter Instruments, Novato,
114 CA) using a P1000 puller (Sutter Instruments) and were filled with (in mM): 130 KCl, 1 MgCl2,
115 0.07 CaCl2, 10 HEPES, 0.1 EGTA (pH-adjusted to 7.3 with KOH, osmolarity 300 mOsm).
116 Pipettes had a 3-4 MΩ tip resistance. Gramicidin (dissolved in DMSO) was added to prefiltered
117 internal solution to produce a final concentration of 5 μg/ml and sonicated for 30 seconds. For
118 one set of experiments (see **Fig. 6**) a CsCl internal pipette solution, containing (in mM): 132
119 CsCl, 10 HEPES, 0.5 EGTA, 2 $MgCl_2$, 0.16 $CaCl_2$ and 5 QX-314 (pH-adjusted to 7.3 with KOH,
120 osmolarity 295 mOsm) was utilized (Sun et al., 2012).

121 High resistance (>0.8 GΩ) cell-attached seals were obtained through the application of
122 negative pressure. Changes in access resistance due to gramicidin pore formation were
123 monitored by repeatedly delivering 20 mV hyperpolarizing voltage steps. Access resistance was
124 measured from the transient responses to the applied voltage steps using established methods
125 (Ulrich and Huguenard, 1997). Appropriate pore formation was indicated by access resistance
126 measurements of 50-100 MΩ, typically achieved within 10-40 minutes. Rapid drops in access
127 resistance at any point during these experiments were indicative of a ruptured membrane patch
128 and these recordings were discarded. The $GABA_A$ receptor agonist muscimol (Abcam,
129 Cambridge, MA) was dissolved in aCSF (100 μM) and applied through a patch pipette adjacent
130 to the cell body of the recorded neuron using 10 ms pressure puffs (Picospritzer III). Membrane
131 potentials were all corrected for the voltage drop across the series resistance.

JNeurosci Accepted Manuscript

132 Data were acquired in pClamp software (Molecular Devices, Sunnyvale, CA) using a
133 Multiclamp 700B amplifier (Molecular Devices), low-pass filtered at 2 kHz, and digitized at 10
134 kHz (Digidata 1440A, Molecular Devices). Data analysis was performed using custom written
135 scripts in MATLAB (MathWorks, Natick, MA).
136
137 *Calcium imaging.* As with the electrophysiology experiments described above, acute brain slices
138 were prepared from P10-20 animals that received an ICV injection of
139 AAV9.Syn.GCaMP6s.WPRE.SV40 at P0-2. Recordings were performed at 31-33°C in aCSF
140 containing: kynurenic acid (3 mM), CGP 55845 (100 nM), and TTX (1 μM). Illumination was
141 provided by a DG-4 arc lamp (Sutter) using a 470 ± 22 nm bandpass excitation filter. Images
142 were acquired with HCImage software (Hamamatsu) at 10 Hz using a 10x/NA0.2 lens. Chemical
143 stimuli were applied with a custom built local perfusion system, which enabled controlled
144 delivery of aCSF with added 5 μM muscimol or 10mM KCl to the field of imaged RT neurons.
145 Images were analyzed off-line, using custom written scripts in MATLAB to measure changes in
146 image intensity within user defined ROIs.
147
148 *Drugs and solutions.* All drugs used were applied in aCSF. VU0463271 (N-Cyclopropyl-N-(4-
149 methyl-2-thiazolyl)-2-[(6-phenyl-3-pyridazinyl)thio]acetamide, Bio-techne, Minneapolis, MN) was
150 diluted from a 10 mM stock in DMSO to a concentration of 10 μM in aCSF. A 50 U/ml stock of
151 Chondroitinase ABC (ChABC, Sigma Aldrich, St. Louis, MO) was made in 0.1% BSA and
152 diluted down to 0.4 U/ml in aCSF.
153
154 *Histochemistry.* At P5, 10, 15, 20 and 40, animals were deeply anesthetized with pentobarbital
155 and transcardially perfused with PBS, followed by ice-cold 4% PFA in PBS (both pH 7.4). Brains
156 were post-fixed overnight in 4% PFA at 4°C. Horizontal sections (40 μm) containing the
157 thalamus were obtained using a vibratome (VT1000S, Leica Biosystems). Free-floating sections

JNeurosci Accepted Manuscript

158 were washed in PBS and then treated with 0.1% sodium borohydride in PBS for 15 minutes to
159 reduce autofluorescence. Sections were washed with PBS, blocked with 2% normal goat serum
160 and Fab fragment of goat anti-mouse IgG (1:500, Jackson ImmunoResearch, West Grove, PA)
161 in PBS for 4 hours at room temperature, and then washed with PBS. Sections were incubated
162 overnight at 4°C with combined primary antibodies for either KCC2 and parvalbumin (rabbit anti-
163 KCC2, 1:500, EMD Millipore, Billerica, MA; mouse anti-parvalbumin, 1:2000, Sigma Aldrich), or
164 parvalbumin and fluorescein labeled Wisteria floribunda agglutinin (1:2000, Vector Laboratories,
165 Burlingame, CA) in PBS with 1% normal goat serum. Sections were washed in PBS and then
166 incubated overnight at 4°C with appropriate combinations of secondary antibodies (donkey α-
167 mouse AF488 and donkey α-rabbit Cy3 for KCC2 labeling, donkey α-mouse Cy3 for WFA
168 labeling; all 1:200 in PBS with 1% normal goat serum, Jackson ImmunoResearch). Sections
169 were washed in PBS and mounted with Vectashield (Vector Laboratories).
170 A subset of histochemical experiments were performed in 300 μm sections prepared as
171 described for use in electrophysiological experiments. Horizontal sections were then bisected
172 and one hemisphere was incubated at 37°C in 0.4 U/ml ChABC, while the other hemisphere
173 was incubated in aCSF. These sections were then post-fixed in 4% PFA for 12 hours before
174 being stained for parvalbumin and WFA as described above.
175 All images were obtained with a Neurolucida system (MicroBrightfield, Colchester, VT) with
176 an Axioskop microscope driven stage and an AxioCam MRc camera (Zeiss Microscopy). All
177 staining and imaging was performed in batches where a set of sections representing all age
178 groups were processed simultaneously. This allowed for us to control for between experiment
179 variability in measured labeling. Images were analyzed using custom written scripts in MATLAB,
180 which allowed for evaluation by two independent, blinded, investigators.
181
182 *Computational modeling.* This model was based on those of Sohal et al. (2003) and Jedlicka et
183 al. (2011). Simulated networks contained 100 RT cells, each of which was modeled as a single

JNeurosci Accepted Manuscript

184 compartment. All simulations were run using NEURON (Hines and Carnevale, 1997) at a
185 temperature of 31°C and with a time step of 0.1 ms.

186 *Intrinsic properties.* Each RT cell consisted of a cylinder with a length of 20 μm and a
187 diameter of 10 μm, based on the dimensions of neurons observed during our
188 electrophysiological experiments. All cells had the following properties: (1) a specific membrane
189 capacitance of 1 μF/cm^2, (2) an axial resistivity of 100 Ω·cm (Destexhe et al., 1996), (3) a leak
190 current with a reversal potential of -70 mV and a conductance that was randomly selected from
191 a uniform distribution between 45 and 55 μS/cm^2 (Sohal and Huguenard, 2003), (4) Na^+ and K^+
192 currents underlying action potentials (I_{Na}, I_K), (5) a low-threshold Ca^{2+} current (I_{Ts}), and (6) a
193 Ca^{2+}-dependent K current (I_{KCa}), and (7) a $GABA_A$ receptor-mediated current comprising a Cl^-
194 current (I_{Cl}) and a nonspecific current that represents HCO_3^- flow (I_{HCO3}). Kinetics and details for
195 I_{Na}, I_K, I_{Ts}, I_{KCa} and the kinetics of intracellular Ca^{2+} ($[Ca^{2+}]_i$) were taken from Sohal et al. (2003).
196 The following changes were implemented: (1) the K^+ reversal potential was fixed at -104 mV, (2)
197 the spike threshold was set to -47 mV (Muñoz and Fuentealba, 2012), and (3) I_{Ts} followed the
198 constant field equation with permeability $p_{Ts} = 10^{-4}$ cm/s. Properties of I_{Cl} and I_{HCO3} were taken
199 from Jedlicka et al. (2011), except for the following: (1) extracellular Cl^- concentration was set to
200 130.5 mM, (2) the conductance ratio g_{Cl}:g_{HCO3} was 4:1, and (3) the peak $GABA_A$ conductance
201 (g_{peak}) per synapse was set to 2.5 nS, or up to 20 nS per cell.

202 *Chloride dynamics.* Kinetics of $[Cl^-]_i$ were adapted from Jedlicka et al. (2011). $[Cl^-]_i$ was
203 computed in a submembrane compartment with a depth of 0.5 μm, allowed to diffuse radially
204 with a diffusion coefficient of 2 μm^2/ms, and was actively extruded (representing the action of
205 KCC2) via Michaelis-Menten kinetics. The dissociation constant (K_d) of Cl^- extrusion was 15 mM
206 and the maximum flux was computed by: $V_{max} = (Cl_\infty + K_d) / \tau_{KCC2}$. In this equation, Cl_∞ (the
207 steady-state value of $[Cl^-]_i$) was 8 mM. A range of values (4-64 sec) for τ_{KCC2} (the extrusion time

JNeurosci Accepted Manuscript

208 constant when $[Cl^-]_i \approx Cl_\infty$) were examined. A constant Cl^- leak current balanced the steady-state
209 extrusion rate.
210 *Network architecture*. RT cells were organized in a simple, linear array. All connections
211 were local and topographic, such that each RT cell projected to the eight nearest RT cells
212 (Sohal and Huguenard, 2003). An action potential was counted when the membrane voltage
213 reached 0 mV. Following a synaptic delay of 1 ms, $GABA_A$ receptors were activated according
214 to kinetics described in Jedlicka et al. (2011). The rise and decay time constants of $GABA_A$
215 currents were 0.1 ms and 50 ms, respectively, and the baseline $GABA_A$ reversal potential was
216 set to -62 mV, based on our data (see **Fig. 2C**).
217 *Simulation protocol.* In each simulation, the network was allowed to initially equilibrate for 3
218 seconds. Following this period, action potential activity was elicited in three central cells (Cells
219 46, 51 and 56) by applying brief (100 µs, 4 nA) and repetitive current pulses. In stimulated cells
220 p_{Ts} and g_{KCa} (conductance of I_{KCa}) were set to zero to better control firing behavior. We tested a
221 range of stimulation frequencies (1-60 Hz), delivered for a total duration of 200 seconds. Total
222 simulation duration was 233 seconds.
223
224 *Experimental design and statistical analysis.* Throughout this study, measurements from
225 neurons in the ventrobasal (VB) thalamic nuclei were used as controls for observations from RT
226 neurons. All histochemical experiments were performed in brain slices from 4 rats and 4 mice
227 per age group (2 male, 2 female; both hemispheres from ~3 slices per animal were analyzed).
228 The number of recordings for basal measures of E_{GABA} (RT: 7 male, 6 female; VB: 7 male, 7
229 female) and Cl^- extrusion (RT: 6 male, 5 female; VB: 7 male, 8 female) reflect the number of
230 animals used, with recordings from RT and VB neurons at times occurring within the same
231 subject.
232 When possible, drug-induced effects were compared against baseline recordings in the
233 same neuron. Each recording of the impact of VU0463271 on basal E_{GABA} (RT: 3 male, 2

JNeurosci Accepted Manuscript

234 female; VB: 1 male, 4 female), basal E_{GABA} when using a Cs-based recording solution (RT: 4
235 male, 1 female; VB: 3 male, 2 female) and Cl^- extrusion (RT: 2 male, 4 female; VB: 4 male, 4
236 female) reflects an independent subject, except where recordings from RT and VB neurons
237 occurred within brain slices of the same animal.

238 The time course of ChABC experiments prohibited pre- and post-treatment recordings from
239 the same neuron, so control recordings were obtained from sham-treated neurons. Each
240 measure of the impact of ChABC treatment on basal E_{GABA} (RT control: 3 male, 5 female; RT
241 ChABC: 4 male, 3 female; VB control: 3 male, 7 female; VB ChABC: 4 male, 3 female), Cl^-
242 extrusion (RT control: 2 male, 2 female; RT ChABC: 1 male, 2 female; VB control: 4 male, 1
243 female; VB ChABC: 2 male, 2 female) and basal E_{GABA} when combined with VU0463271 (RT
244 control: 4 male, 4 female; RT ChABC: 2 male, 2 female) reflects the number of animals used,
245 with recordings from RT and VB neurons at times occurring within the same subject. Control
246 and ChABC treated recordings were always performed in different brain slices.

247 In calcium imaging experiments, muscimol and elevated KCl responses were evaluated in
248 each brain slice, with the KCl treatment being a positive control for the change in fluorescence
249 associated with a mild depolarization. For evaluating the overall distribution of responses, the
250 change in fluorescence of each detected RT neuron was compared (Muscimol: 1772; KCl:
251 1728). Photobleaching and shifting tissue, among other factors, result in a differing number of
252 detectable cells in experiments performed in the same brain slice. The typical response to
253 muscimol and elevated KCl was evaluated by comparing the median change in fluorescence
254 that a treatment evoked within each subject (5 male, 2 female, average of 1.7 slices per animal).
255 Similar comparisons were made in experiments where brain slices were preincubated in
256 VU0463271 prior to calcium imaging (Muscimol+VU0463271: 1772 cells; KCl+VU0463271:
257 1728 cells; 3 male, 3 female, average of 1.8 slices per animal).

258 All statistical tests were performed in MATLAB. Unless otherwise noted, statistical tests to
259 determine the significance of differences between groups were performed using unpaired or

JNeurosci Accepted Manuscript

260 paired Student's t-test. When utilized, ANOVA tests were followed by a *post hoc* Tukey's HSD
261 analysis. Comparisons requiring a nonparametric factorial analysis were calculated using a two-
262 way Aligned Rank Transform ANOVA (Wobbrock et al., 2011). This method independently rank
263 transforms the data to separate the contributions of the main effects and interactions. After the
264 data has been aligned and ranked, a regular parametric ANOVA with Tukey's HSD *post hoc*
265 testing can be used to analyze each individual effect. Group measures are presented as mean ±
266 SEM. The threshold for differences to be considered significant was set at $p<0.05$.
267
268 **Results**

269 The goal of our study was to resolve how intracellular Cl^- is regulated in the RT nucleus, a
270 structure proposed to serve as an important seizure choke point. We used anatomical and
271 functional approaches to determine the relative contributions of KCC2 and impermeant anions
272 to setting basal $[Cl^-]_i$ in RT neurons. We also assessed the degree to which these two
273 mechanisms define the activity-dependent, Cl^- extrusion capacity of RT neurons. Finally, we
274 incorporated our observations into a computational model of a local RT network to better
275 understand how seizure activity propagation within this network might depend on the properties
276 of Cl^- regulation. Collectively, our experimental and computational results suggest that the weak
277 Cl^- extrusion capacity of RT neurons is sufficient to support basal inhibitory, GABAergic
278 signaling, but that the nucleus is susceptible to an activity-dependent switch from synaptic
279 inhibition to excitation.
280

281 **KCC2 expression is low, but present in RT neurons**

282 As a major Cl^- transporter in the central nervous system, KCC2 is thought to critically maintain
283 the low $[Cl^-]_i$ that enables inhibitory, $GABA_A$ receptor-mediated signaling in adult neurons (Kaila
284 et al., 2014). Interestingly, the RT nucleus is one of only a small number of regions in the adult
285 rat brain with minimal KCC2 mRNA expression (Kanaka et al., 2001). Reduced expression of

JNeurosci Accepted Manuscript

286 KCC2 protein is also observed in the RT nucleus of adult rats (Barthó et al., 2004) and mice
287 (Sun et al., 2012). Anatomical assays primarily served as the basis for these previous
288 measures.

289 The developmental upregulation of KCC2 in most brain regions is well-established (Kaila et
290 al., 2014). However, to our knowledge, this phenomenon has not been examined in the
291 thalamus. Therefore, we began our study by measuring KCC2 immunoreactivity within the
292 rodent thalamus as a function of age (P5-40) (**Fig. 1**). To control for experimental variability, we
293 concurrently performed immunohistochemistry on sets of brain slices representing all age
294 groups. As in other brain structures, thalamic KCC2 immunoreactivity increased with age in the
295 rats we examined ($F(4,146)=2.60$, $p=0.038$, $n=4$, two-way ANOVA, **Fig. 1B**). Specifically, overall
296 KCC2 immunoreactivity was low throughout the thalamus of P5 rats (21.3 ± 1.3 A.U.), and
297 increased thereafter (P20 rats: 47.4 ± 8.7 A.U., $p=0.049$; P40 rats: 47.4 ± 6.0 A.U., $p=0.033$).
298 While immunoreactivity in both the ventrobasal (VB) thalamus and RT nucleus increased with
299 age, the effect was blunted in RT. These results suggest that KCC2 is expressed in the adult rat
300 RT nucleus, albeit at relatively lower levels than observed in VB thalamus ($F(1,146)=8.37$,
301 $p=0.0044$, $n=4$, two-way ANOVA). We detected a similar pattern of KCC2 staining in P10-40
302 mice (**Fig. 1B**).

303 In addition to gross, age-dependent differences in KCC2 immunoreactivity, we also
304 observed that the distribution of KCC2 expression was not even throughout RT, particularly in
305 adult rats and mice. To quantify KCC2 immunoreactivity, we drew a linear ROI that extended
306 from the anterior-most edge to the lateral-most edge of the RT nucleus (see lower left panel in
307 **Fig. 1A**). This line bisected the RT nucleus, and then automatically expanded to a width of 75
308 μm. This linear ROI was further subdivided into 10 equal segments that were numbered from 1
309 (anterior-most) to 10 (lateral-most, see **Fig. 1C**). The mean fluorescence intensity within each
310 segment was calculated.

JNeurosci Accepted Manuscript

311 We quantified KCC2 immunoreactivity in each segment along the anterior-to-lateral axis, 312 relative to the mean intensity level across all RT segments of each slice (**Fig. 1D**), an approach 313 to account for slice-to-slice staining variability. When expression was quantified in this manner 314 in P40 rats, we observed that KCC2 levels were not uniform across segments of the RT nucleus 315 ($F(10,200)=39.4$, $p<0.001$, n=4, one-way ANOVA). This finding establishes that KCC2 316 immunoreactivity varies according to location within the RT nucleus. To discern specific 317 immunoreactive differences among the segments, we compared individual segment means to 318 the overall mean across all RT segments.

319 Relative to the overall RT mean, KCC2 immunoreactivity was elevated in the two anterior-320 most segments of the adult rat RT nucleus (segment 1: 134±5.5%, $p<0.001$; segment 2: 321 120±3.3%, $p<0.001$), as well as in the lateral-most segment (segment 10: 116±3.6%, $p=0.004$). 322 Centrally-located segments, on the other hand, had much reduced KCC2 immunoreactivity 323 (segment 6: 82±2.5%, $p<0.001$; segment 7: 79±2.6%, $p<0.001$, segment 8: 81±3.1%, $p<0.001$).

324 Next, we applied the aforementioned approach to younger, P10 rats. Although KCC2 levels 325 varied minimally along the extent of the RT nucleus in P10 rats ($F(10,144)=2.35$, $p=0.013$, n=4, 326 one-way ANOVA), no significant differences relative to the overall RT mean were observed. 327 These results suggest that there is greater regional variability in KCC2 immunoreactivity in the 328 RT nucleus of P40 rats than of P10 rats. We observed a broadly similar pattern of KCC2 329 immunoreactivity in mice (**Fig. 1D**).

330 Collectively, our results indicate that KCC2 expression is consistently lower in RT neurons 331 than VB neurons throughout the first few postnatal weeks, in agreement with prior reports 332 (Kanaka et al., 2001; Barthó et al., 2004; Sun et al., 2012). However, it remained unclear the 333 extent to which detected immunoreactivity in the RT nucleus was due to KCC2 protein 334 expression or non-specific labeling. Therefore, we decided to use functional measurements to 335 assess whether diminished KCC2 reduces the capacity of RT neurons to maintain a low $[Cl^-]_i$.

JNeurosci Accepted Manuscript

336

337 **$[Cl^-]_i$ is relatively low in RT neurons**

338 Based on our observation that KCC2 immunoreactivity is low in RT neurons, we expected to
339 find elevated $[Cl^-]_i$ in these neurons. If true, then GABAergic signaling in RT neurons would likely
340 be excitatory. To assess $[Cl^-]_i$ in RT neurons without perturbing the intracellular Cl^- gradient, we
341 performed gramicidin perforated patch recordings in RT neurons of P10-20 rats.

342 Successful patch perforation was indicated when access resistance measurements
343 reached 50-100 MΩ. Neurons were voltage-clamped at -70 mV and then stepped to a command
344 potential between -110 and -20 mV for 2.5 sec of each 15 sec sweep. These 10 voltage steps
345 were given in a randomized in order to reduce experimentally-induced Cl^- loading. The $GABA_A$
346 receptor agonist muscimol (100 μM) was pressure-applied to the soma of the voltage-clamped
347 neuron for 10 ms during each voltage step. We adjusted the pressure used for agonist
348 application so that GABA-evoked currents fully decayed within 2 sec from application.

349 Current-voltage (I-V) relationships were plotted for both the leak current and the muscimol-
350 induced current, and the voltage at which these currents was equal indicated the reversal
351 potential for the GABA-induced current (E_{GABA}). E_{GABA} is largely determined by E_{Cl}, with E_{HCO}
352 (the reversal potential for bicarbonate ions) providing a smaller contribution (Bormann et al.,
353 1987; Staley et al., 1995). We did not isolate the relative contributions of E_{Cl} and E_{HCO} to E_{GABA}
354 in our recordings, so our calculations may slightly overestimate the $[Cl^-]_i$ of RT neurons (Staley
355 et al., 1995). We corrected all measurements for the voltage drop across the series resistance.

356 We determined that RT neurons have an E_{GABA} of -62±3.0 mV (n=13, **Fig. 2A,C**). For
357 comparison, E_{GABA} was also measured in VB neurons, where it was found to be significantly
358 more hyperpolarized than in RT neurons (-79±2.7 mV, t(25)=4.15, p<0.001, n=14, **Fig. 2B,C**).
359 Based on our recording solutions, $[Cl^-]_i$ was ~12 mM in RT neurons and ~6 mM in VB neurons.
360 Interestingly, while we measured a very consistent E_{GABA} in the majority of VB neurons, this

JNeurosci Accepted Manuscript

361 parameter was more variable among RT neurons. The RT nucleus contains a heterogeneous
362 population of neuronal subtypes, associated with distinct functional characteristics (Lee et al.,
363 2007; Halassa et al., 2014; Clemente-Perez et al., 2017), and may provide a source of this
364 variability. Our electrophysiological recordings were targeted to the central section of the RT
365 nucleus, and likely include both parvalbumin- and somatostatin-positive RT neuron subtypes
366 (Clemente-Perez et al., 2017).

367 While gramicidin perforated patch recordings are designed to maintain physiological $[Cl^-]_i$ in
368 neurons, the low experimental yield afforded by this technique limits the ability to make
369 observations in large populations of neurons. Therefore, we also examined the response of RT
370 neurons to $GABA_A$ receptor stimulation using GCaMP6s-based calcium imaging. Acute brain
371 slices, where GCaMP6s had been virally transfected into RT neurons, were prepared and a
372 local perfusion system was used to deliver test compounds in proximity to the RT nucleus (**Fig.
373 2D**). Cell-intrinsic responses to muscimol stimulation were isolated by blocking AMPA, NMDA
374 and $GABA_B$ receptors, as well as voltage-gated sodium channels. A two minute application of
375 muscimol (5µM) caused a decrease in the fluorescence of most, but not all, RT neurons (**Fig.
376 2E,G**). However, subsequently depolarizing the RT neurons with the addition of 10 mM KCl
377 (12.5 mM in total) for two minutes induced a robust increase in fluorescence (**Fig. 2F,G**). Based
378 on E_K measurements of RT neurons (McCormick and Prince, 1986), the high-K^+ test solution
379 should depolarize neurons to around -45 mV. Compared across animals, 10 mM KCl produced
380 a significantly greater median increase in fluorescence (22.3%, interquartile range 12.1–42.7%,
381 n=1728 cells, n=7 animals, **Fig. 2G**) than the mild decrease following muscimol stimulation
382 (-2.8%, interquartile range -7.1–4.8%, n=1772 cells, n=7 animals, Z=44.86, $p<0.001$, Wilcoxon
383 rank sum test).

384 Because KCC2 immunoreactivity is reduced in the RT nucleus, the observation that $[Cl^-]_i$
385 remained low — and GABAergic signaling remained inhibitory — in most RT neurons was
386 unexpected. Considering that KCC2 immunoreactivity was low in the RT nucleus (see **Fig.** 1),

JNeurosci Accepted Manuscript

387 we were motivated to determine if extracellular impermeant anions ($[A]_o$) contribute to Cl^-
388 regulation in RT neurons (Glykys et al., 2014a).
389

390 **While elevated in RT neurons, $[A]_o$ contribute only mildly to setting E_{GABA}**

391 Chondroitin sulfate proteoglycans (CSPGs) are major extracellular matrix proteins that contain
392 abundant, negatively charged, sulfate groups, thus making them a significant source of $[A]_o$
393 (Bandtlow and Zimmermann, 2000; Glykys et al., 2014a). The disaccharide formed by
394 *N*-acetylgalactosamine and glucuronic acid is bound by the plant lectin *Wisteria floribunda*
395 agglutinin (WFA), and therefore can be used to label chondroitin sulfate glycosaminoglycan
396 elements of CSPGs (Horii-Hayashi et al., 2015). WFA staining showed that the CSPGs
397 surrounding RT neurons increase during development from P5-40 (**Fig. 3**).

398 We first examined the overall levels of WFA fluorescence in the thalamus across the
399 different ages of rats we tested. As with KCC2 immunoreactivity, WFA stain intensity increased
400 with age ($F(4,218)=14.48$, $p<0.001$, n=4, two-way ANOVA, **Fig. 3B**). While overall WFA levels
401 were initially low throughout the thalamus of P5 rats (25.0±1.8 A.U.), overall WFA staining was
402 elevated in P20 rats (49.7±7.0 A.U., $p=0.0011$) and further increased by P40 (72.7±7.6 A.U.,
403 $p<0.001$). This observation is consistent with prior findings showing that WFA staining first
404 appears between P7-14 in many regions of the mouse brain and further increases as the
405 extracellular matrix matures during the next few weeks of development (Horii-Hayashi et al.,
406 2015). Across the ages we evaluated, there was greater mean WFA staining throughout the RT
407 nucleus (57.6±3.4 A.U., n=20), relative to mean levels in VB (39.9±2.6 A.U., n=20,
408 $F(1,218)=16.31$, $p<0.001$, n=4, two-way ANOVA). Intense WFA staining of white matter tracts is
409 likely non-specific as it is not eliminated by enzymatic reduction of CSPGs (Ajmo et al., 2008,
410 see **Fig. 4F**). An overall similar pattern of WFA staining was likewise detected in P10-40 mice
411 (**Fig. 3**).

JNeurosci Accepted Manuscript

412 As with measurements of KCC2 immunoreactivity (see **Fig. 1D**), WFA staining was also
413 evaluated in a linear ROI that extended from the anterior-most edge to the lateral-most edge of
414 the RT nucleus, and was then subdivided into 10 equal segments (see lower left panel in **Fig.**
415 **3A**, **Fig. 1C**). We calculated the mean fluorescence intensity within each segment.

416 When WFA labeling in each segment along the anterior-to-lateral axis was compared to the
417 mean intensity across all of RT, we found that WFA levels were not uniform across segments of
418 the RT nucleus of P10 rats ($F(10,202)=9.82$, $p<0.001$, $n=4$, one-way ANOVA, **Fig. 3C**). Relative
419 to the mean WFA intensity within RT, WFA staining was increased in a central segment of RT
420 (segment 6: 119±5.5%, $p=0.0047$). We also observed that WFA intensity varied along the extent
421 of the RT nucleus in P40 rats ($F(10,254)=5.49$, $p<0.001$, $n=4$, one-way ANOVA). There was
422 reduced WFA staining in the anterior-most segment of the RT nucleus (segment 1: 86±3.6%,
423 $p=0.0046$) relative to the mean WFA intensity within RT.

424 Considering that RT neurons maintain a surprisingly low $[Cl^-]_i$, despite the low expression of
425 KCC2 in the RT nucleus, we next tested the hypothesis that elevated CSPGs surrounding RT
426 neurons (as indicated by our WFA staining) provide a compensatory mechanism of $[Cl^-]_i$
427 regulation. Therefore, we measured the impact of reducing $[A]_o$ surrounding RT neurons in P10-
428 20 rats. The enzyme chondroitinase ABC (ChABC) digests the chondroitin sulfate
429 polysaccharide elements of CSPGs (Yamagata et al., 1968) and releases negatively charged
430 sulfate groups, thereby reducing $[A]_o$ (Glykys et al., 2014a). We measured changes in E_{GABA}
431 between neurons incubated in ChABC (0.4 U/ml, 37°C) for 2 hours and control neurons
432 incubated in the absence of ChABC.

433 Using perforated patch recordings, we found that the initial E_{GABA} measurement in ChABC-
434 treated RT neurons (-63±3.2 mV, $n=7$, **Fig. 4A**) was unchanged from control RT neurons (-
435 60±2.9 mV, $t(13)=0.66$, $p=0.52$, $n=8$, **Fig. 4C**). Likewise, the initial E_{GABA} measurement in
436 ChABC-treated VB neurons (-70±5.4 mV, $n=7$, **Fig. 4B**) was no different from control VB

JNeurosci Accepted Manuscript

437 neurons, (-74 ± 2.1 mV, $t(15)=0.69$, $p=0.50$, $n=10$, **Fig. 4C**). While the initial measurement of
438 E_{GABA} was not different between ChABC-treated and control RT neurons, we observed an effect
439 of ChABC treatment when E_{GABA} measurements were repeated at 2.5 minute intervals over a 15
440 minute period ($F(1,68)=8.74$, $p=0.0043$, $n=7,7$, two-way ANOVA, **Fig. 4D**). Across all time
441 points, ChABC-treated RT neurons underwent a greater, average shift in E_{GABA} ($\Delta+3.3\pm0.7$ mV,
442 $n=7$) than control neurons ($\Delta+0.2\pm0.8$ mV, $n=7$). The impact of ChABC treatment on the E_{GABA}
443 of RT neurons was particularly evident at 12.5 minutes (control: $\Delta+0.9\pm3.4$ mV, $n=7$; ChABC-
444 treated: $\Delta+8.1\pm1.9$ mV, $n=7$). There was no effect of either ChABC treatment ($F(1,82)=1.94$,
445 $p=0.17$, $n=7,9$, two-way ANOVA) or time ($F(5,82)=0.57$, $p=0.72$, $n=7,9$, two-way ANOVA) on the
446 E_{GABA} of VB neurons (**Fig. 4E**). The modest effect of ChABC treatment on E_{GABA} motivated us to
447 evaluate treatment efficacy in an independent manner. Towards this end, we prepared acute
448 brain slices (300 μm) and then treated them in the same, aforementioned manner. However,
449 rather than performing electrophysiological measurements, we performed WFA labeling
450 protocols on control and ChABC-treated slices to localize CSPGs (**Fig. 4F**). We observed that
451 mean RT WFA fluorescence was lower in ChABC-treated (34.3 ± 0.5 A.U.) versus control slices
452 (42.5 ± 1.6 A.U., $t(15)=4.15$, $p=0.0024$, $n=4$, **Fig. 4G**), an effect particularly evident when the
453 change was measured by first normalizing RT fluorescence to adjacent, VB fluorescence levels
454 (control: $25.3\pm3.1\%$; ChABC: $-1.8\pm1.5\%$, $t(15)=6.19$, $p<0.0001$, $n=4$; **Fig. 4H**). This observation
455 confirms that the ChABC treatment protocol utilized in our perforated patch experiments was
456 indeed associated with a significant reduction in $[A]_o$.

457 Collectively, these results indicate that although elevated levels of $[A]_o$ surround RT
458 neurons, perturbing CSPGs only affected Cl^- regulation following prolonged periods of
459 stimulation. Considering that $[A]_o$ did not exert a very large impact on the $[Cl^-]_i$ of RT neurons,
460 we next tested the hypothesis that the apparently low level of KCC2 expression in the RT
461 nucleus nonetheless actively contributes to $[Cl^-]_i$ regulation.

JNeurosci Accepted Manuscript

462

463 **KCC2 is a significant regulator of $[Cl^-]_i$ in RT neurons**

464 Due to the generally low Cl^- flux of resting neurons, it has been proposed that even minimal
465 KCC2 might provide sufficient Cl^- extrusion to maintain a hyperpolarizing E_{GABA} (Blaesse et al.,
466 2009). To determine if the apparently reduced level of KCC2 functionally contributes to
467 maintaining a hyperpolarized E_{GABA} in RT neurons, the selective KCC inhibitor VU0463271
468 (Delpire et al., 2012) was applied during perforated patch recordings in P10-20 rats. While
469 VU0463271 may act on KCCs other than KCC2, brain mRNA levels for KCC1, KCC3 and KCC4
470 are much lower than for KCC2 (Kaila et al., 2014). There is also no sign that KCC1, KCC3 or
471 KCC4 localize within the thalamus (Rivera et al., 1999; Le Rouzic et al., 2006).

472 The addition of VU0463271 (10 μM) produced a clear shift to a more depolarized E_{GABA} in
473 perforated patch recordings of RT neurons (**Fig. 5A**). VU0463271 application produced a time-
474 dependent shift in the E_{GABA} of RT neurons ($F(7,32)=24.25$, $p<0.001$, $n=5$, one-way ANOVA),
475 which first became clear following 5 minutes of treatment with VU0463271 ($\Delta+12\pm1.5$ mV,
476 $p<0.001$, **Fig. 5A2**). Overall, the baseline E_{GABA} (-58 ± 3.4 mV) became more depolarized
477 following 10 minutes of VU0463271 application (-42 ± 5.4 mV, $t(4)=6.24$, $p=0.0034$, $n=5$, paired t-
478 test, **Fig. 5A3**).

479 As in RT neurons, there was a time-dependent shift in the E_{GABA} of VB neurons following
480 VU0463271 application ($F(7,32)=14.38$, $p<0.001$, $n=5$, one-way ANOVA, **Fig. 5B**). This shift in
481 E_{GABA} first became clear following 2.5 minutes of treatment with VU0463271 ($\Delta+9\pm4.4$ mV,
482 $p=0.04$, **Fig. 5B2**). Overall, VU0463271 also depolarized the E_{GABA} of VB neurons (baseline: -
483 69 ± 5.6 mV; post-VU0463271: -52 ± 8.7 mV, $t(4)=7.47$, $p=0.0017$, $n=5$, paired t-test, **Fig. 5B3**). In
484 control experiments, no similar time-dependent shift in E_{GABA} was observed (data not shown),
485 comparable to the minimal change of E_{GABA} observed in control recordings from our ChABC
486 experiments (c.f. **Fig. 4D,E**).

JNeurosci Accepted Manuscript

487 As with our initial measurements of E_{GABA} in RT neurons, we again used calcium imaging to
488 examine responses of larger populations of neurons, now preincubated with VU0463271 (10
489 μM) for 5 minutes prior to the start of recording. Preincubation was necessary because
490 responses evoked by local muscimol perfusion attenuated following multiple rounds of
491 application (data not shown). A two-minute application of muscimol now produced a more varied
492 response, with an increase in fluorescence occurring in most RT neurons (**Fig. 5C**). In
493 aggregate, muscimol stimulation evoked a small, but now positive, 5.5% change in median
494 fluorescence (Interquartile range -4.9–12.4%, n=1722 cells, n=6 animals, **Fig. 5E**). As before,
495 mildly depolarizing VU0463271-preincubated, RT neurons with the addition of 10 mM KCl for
496 two minutes produced a robust increase in fluorescence (22.2%, Interquartile range 16.0–
497 31.1%, n=1732 cells, n=6 animals, Z=35.92, p<0.001, Wilcoxon rank sum test, **Fig. 5D**).
498 When the median calcium imaging response per animal was compared across the four
499 conditions tested (c.f. **Figs. 2E-G** and **5C-E**), larger changes in fluorescence occurred in
500 VU0463271-treated brain slices (15.4±2.5%, n=12) than in controls (10.5±4.6%, n=14,
501 F(1,22)=4.76, p=0.040, two-way Aligned Rank Transform ANOVA, **Fig. 5F**). The response to a
502 mild depolarization with KCl was very similar between control (23.1±5.9%, n=7) and VU0463271
503 pretreated brain slices (22.6±2.1%, n=6). Therefore, the observed treatment effect is likely due
504 to the difference in the muscimol-induced change in fluorescence between control (-2.0±1.4%,
505 n=7) and VU0463171 pretreated brain slices (8.2±1.9%, n=6). The impact of VU0463271 on
506 muscimol-induced responses is consistent with the depolarizing E_{GABA} shift we observed in
507 VU0463271-treated RT neurons.
508 As we have found that either inhibiting KCC2 or reducing $[A]_o$ depolarizes the E_{GABA} of RT
509 neurons, we now sought to assess the interaction of these two mechanisms in regulating $[Cl^-]_i$.
510 Similar to prior experiments, we applied VU0463271 during perforated patch recordings from
511 P10-20 rats in brain slices that were either incubated in ChABC (0.4 U/ml, 37°C) for 2 hours or

JNeurosci Accepted Manuscript

512 control slices incubated in the absence of ChABC (**Fig. 5G**). We found that the average change
513 in E_{GABA} measured in ChABC-treated neurons (Δ+7.7±1.2 mV), across all times of VU0463271
514 exposure, was larger than in control-treated neurons (Δ+5.4±0.6 mV, $F(1,100)=5.66$, $p=0.020$,
515 n=4,8, two-way ANOVA). This observation suggests that VU0463271 and ChABC treatment act
516 through distinct molecular mechanisms.

517 While VU0463271 is thought to specifically antagonize the KCCs, we sought to validate the
518 role of KCC2 in RT neurons using an additional method. Intracellular Cs^+ is known to effectively
519 reduce the ability of KCC2 to extrude Cl^- (Williams and Payne, 2004). Therefore, rather than the
520 KCl-based recording pipette solution we used in prior experiments, we now utilized a CsCl-
521 based solution. Recordings from RT neurons using the aforementioned CsCl internal solution
522 revealed a more depolarized E_{GABA} during the five minutes of baseline recording (-54±2.9 mV,
523 **Fig. 6A**) than found when using a KCl pipette solution (c.f. Figure 2C). The depolarized reversal
524 potential observed using a Cs-based internal solution appears to result from the blockade of
525 KCC2, because subsequent application of VU0463271 (10 μM) produced no significant, time-
526 dependent shift in E_{GABA} ($F(7,31)=0.62$, $p=0.74$, n=5, one-way ANOVA, **Fig. 6A2**). Thus,
527 VU0463271 had little overall effect on the E_{GABA} of RT neurons (-45±4.5 mV, n=5, $t(4)=1.72$,
528 $p=0.16$, paired t-test, **Fig. 6A3**).

529 Similar to RT neurons, the baseline E_{GABA} of VB neurons was less hyperpolarized when
530 recorded with a CsCl internal solution (**Fig. 6B**). Nonetheless, we observed a small, time-
531 dependent shift in E_{GABA} in response to application of VU0463271 ($F(7,31)=16.92$, $p=0.0025$,
532 n=5, one-way ANOVA) following 7.5 minutes of treatment (Δ+5±1.1 mV, $p=0.011$, **Fig. 6B2**).
533 Overall, the baseline E_{GABA} (-69±1.4 mV) became more depolarized following 10 minutes of
534 VU0463271 application (-65±1.0 mV, $t(4)=4.74$, $p=0.009$, n=5, paired t-test, **Fig. 6B3**). The
535 ability to still detect VU0463271 sensitivity may reflect a greater resiliency of VB neurons to the
536 impact of a Cs-based internal solution on KCC2 function.

JNeurosci Accepted Manuscript

537 Together, these findings suggest that the KCC2 expressed in the RT nucleus still
538 contributes significantly to maintaining a relatively low baseline $[Cl^-]_i$, which in turn supports
539 inhibitory responses to GABAergic signaling in RT neurons. However, it remains possible that
540 reduced KCC2 expression diminishes the capacity of RT neurons to maintain a low $[Cl^-]_i$ during
541 intense periods of GABAergic signaling.
542
543 **RT neurons have a diminished ability to recover from Cl^- loading**
544 While RT neurons express sufficient levels of KCC2 to maintain a low basal $[Cl^-]_i$, it remains
545 unclear how relatively limited KCC2 expression impacts the responses of RT neurons to more
546 intense periods of GABAergic signaling. In the cortical undercut model, a reduction in KCC2
547 expression is not accompanied by a shift in basal E_{GABA}, although Cl^- accumulates faster in
548 these neurons during stimulation (Jin et al., 2005). Therefore, we tested the capacity of RT
549 neurons to resist Cl^- loading during repetitive GABAergic signaling, and the rate at which Cl^-
550 extrusion returns E_{GABA} to basal levels once stimulation has ceased.
551 Cl^- loading and recovery was measured using perforated patch recordings where the
552 membrane potential of the neuron was held at -30 mV for 500 ms, and then ramped from -100
553 to -10 mV over a duration of 500 ms (**Fig. 7A**). This voltage-clamp protocol was repeated once
554 per second for 100 seconds. Following a 10 sec period of baseline recording, Cl^- loading was
555 induced with 10, 20 ms puffs of 100 µM muscimol, occurring once every three seconds (**Fig.
556 7A**). Muscimol was applied while the neuron was voltage-clamped at -30 mV to promote Cl^-
557 entry. E_{GABA} was determined by finding the voltage at which the baseline and Cl^- loading current
558 traces intersected, following correction for the voltage drop across the series resistance (**Fig.
559 7B,** a vs. b). Changes in E_{GABA} associated with Cl^- recovery, also determined according to the
560 intersection with baseline current traces (**Fig. 7B**, a vs. c), were measured for 62 sec following
561 the end of Cl^- loading. For each neuron, the time constants for Cl^- loading (τ_{load}) and recovery

JNeurosci Accepted Manuscript

562 (τ_{rec}) were determined by fitting the measured E_{GABA} values during the rising and falling phases,
563 respectively, with single-exponential functions (**Fig. 7C,D**).

564 Our experiments revealed a clear difference in τ_{load} between RT and VB neurons, and
565 indicated that RT neurons are particularly susceptible to Cl^- loading. In general, VB neurons
566 displayed Cl^- loading profiles similar to those previously described (Jin et al., 2005), where the
567 initial E_{GABA} measurement at the start of loading was comparable to the final E_{GABA} at the end of
568 recovery (ΔE_{GABA}: -2.0±2.0 mV, n=16, **Fig. 7D,E**). The insets in **Fig. 7C-D** illustrate how this
569 measurement was calculated. In contrast to VB neurons, RT neurons displayed a flat Cl^- loading
570 profile and the E_{GABA} measured at the end of recovery was substantially below the initial
571 measurement (ΔE_{GABA}: -17.3±3.3 mV, n=11, $t(25)=3.81$, $p<0.001$, **Fig. 7C,E**). This near-
572 instantaneous τ_{load} is likely due to the initial application of muscimol producing a rapid shift in the
573 E_{GABA} of RT neurons, which then only returns to basal levels following a prolonged recovery; our
574 experimental paradigm promotes large Cl^- influxes by applying muscimol while neurons are
575 highly depolarized (see **Fig. 7A**). While we measured a τ_{load} of 8.5 ± 0.6 sec in VB neurons (data
576 not shown), such measurements were obscured in RT neurons by the rapid dynamics of Cl^-
577 loading.

578 Consistent with the limited Cl^- extrusion capacity of RT neurons revealed by our Cl^- loading
579 measurements, the τ_{rec} for RT neurons (30.3±3.7 sec, n=11) was significantly slower than in VB
580 neurons (18.3±2.3 sec, n=15, $t(24)=2.89$, $p=0.008$, **Fig. 7F**). As with our earlier measurements
581 of basal E_{GABA}, we next investigated if limited KCC2 nonetheless contributes to Cl^- loading and
582 recovery in RT neurons. Unlike in our basal E_{GABA} measurements, application of the KCC2
583 antagonist VU0463271 did not produce a shift in the τ_{rec} of RT neurons between baseline
584 (25.5±3.3 sec) and 10 minute post-VU0463271 (10 μM) measurements (27.2±3.1 sec, n=6,
585 $t(5)=0.77$, $p=0.47$, paired t-test, **Fig. 7G**). In contrast, we observed that the τ_{rec} for VB neurons

JNeurosci Accepted Manuscript

586 became slower following 10 minutes of VU0463271 treatment (16.4±3.6 sec vs. 28.2±4.0 sec,
587 n=8, t(7)=2.44, p=0.045, paired t-test, **Fig. 7H**).

588 We also assessed the impact of reducing $[A]_o$ on the speed of recovery from Cl^- loading.
589 The τ_{rec} for RT neurons incubated in ChABC (0.4 U/ml, 37°C) for 2 hours (32.8±4.4 sec, n=3)
590 was unchanged from control RT neurons that were incubated in the absence of ChABC
591 (31.1±6.6 sec, n=4, t(5)=0.19, p=0.86, **Fig. 7I**). We also detected no impact of ChABC
592 incubation on the τ_{rec} of VB neurons (20.4±3.0 sec, n=4), as compared to control VB neurons
593 (23.1±1.6 sec, n=5, t(7)=0.86, p=0.42, **Fig. 7I**).

594 Collectively, these extrusion experiments indicate that RT neurons have a reduced capacity
595 to resist activity-dependent shifts in $[Cl^-]_i$. While VU0463271 was effective in slowing the rate of
596 Cl^- extrusion in VB neurons, we observed no VU0463271 effect on Cl^- extrusion in RT neurons.
597 The lack of VU0463271 sensitivity on Cl^- extrusion in RT may result from low KCC2 expression;
598 that is, KCC2 is likely overwhelmed during substantial chloride loading, thereby mitigating the
599 effects of pharmacological blockade. Due to their lack of efficient Cl^- extrusion mechanisms, RT
600 neurons may be more susceptible to undergoing a shift from inhibitory to excitatory GABAergic
601 signaling during periods of repeated stimulation, such as during a seizure.
602

603 **Low Cl^- extrusion may promote the spread of activity between RT neurons**

604 Although RT neurons maintain a basal $[Cl^-]_i$ that appears to be sufficiently low to support
605 inhibitory GABAergic signaling, reduced levels of KCC2 compromise rapid recovery from Cl^-
606 loading in these neurons. Previous computational models have examined activity-dependent Cl^-
607 accumulation in neurons (Jedlicka et al., 2011), and how even mildly reduced KCC2-mediated
608 Cl^- extrusion disrupts neural coding (Doyon et al., 2015). We expanded upon this prior work by
609 modeling the impact of reduced Cl^- extrusion on signaling within a network of RT neurons. We

JNeurosci Accepted Manuscript

610 developed this model primarily to understand how the RT seizure choke point behaves during
611 low and moderate activity bouts.

612 Based on prior models used to study seizure activity within the RT nucleus (Sohal and
613 Huguenard, 2003), we designed a linear network of 100 RT neurons, in which each cell
614 projected GABAergic synapses to the eight nearest neurons (**Fig. 8A**). To approximate
615 excitatory input to this network, we delivered repetitive, simulated depolarizing current injections
616 to three centrally located neurons in the array (Cells 46, 51 and 56) to evoke action potentials
617 (**Fig. 8B,C1**; e.g., Cell 51). In the example shown here, the three stimulated RT neurons
618 generated action potentials at 30 Hz, and all RT neurons extruded Cl^- with a τ_{rec} of 32 seconds,
619 a value comparable to our experimental results. Evoked action potentials immediately produced
620 GABAergic currents in neurons postsynaptic to the stimulated cell (**Fig. 8C1**; e.g., Cell 53 inset).
621 While each individual postsynaptic potential only generated a transient increase in $[Cl^-]_i$, the
622 slow decay kinetics of IPSCs in RT neurons (Huntsman and Huguenard, 2006), coupled with
623 slow Cl^- extrusion mechanisms in RT neurons, resulted in a fairly steady, activity-dependent,
624 elevation in $[Cl^-]_i$. Once $[Cl^-]_i$ became sufficiently elevated, postsynaptic potentials became
625 suprathreshold and evoked action potentials (**Fig. 8C2**; e.g., cell 53). Thus, as glutamatergic
626 signaling was not present in our model, excitatory GABAergic signaling was sufficient to
627 propagate activity within this simplified network.

628 Next, we examined how varying the τ_{rec} within our model altered the spread of activation.
629 When the τ_{rec} was equal to 32 seconds, 30 Hz stimulation was sufficient to produce activation
630 throughout the network, including neurons more distant from the sites of direct stimulation (**Fig.
631 8C3**; e.g., Cell 80). When we accelerated τ_{rec}, higher frequency stimulation was required to
632 recruit activity within our network (**Fig. 8D**), as KCC2 more effectively offset Cl^- accumulation
633 between postsynaptic potentials. In aggregate, we observed a rapid, τ_{rec}-dependent, inflection
634 point between stimulation frequencies unable to recruit network activity and stimulation

JNeurosci Accepted Manuscript

635 frequencies that triggered activity throughout the entire RT network (**Fig. 8D**). Increasing the
636 stimulation frequency also effectively reduced the latency for distant neurons to begin firing
637 action potentials (**Fig. 8E**). We examined the interplay between τ_{rec} and stimulation frequency
638 on global RT network activity across a range of parameters (**Fig. 8F**). Across this range of
639 parameters, only a narrow band separated conditions that activated zero neurons and all
640 neurons in our network, suggesting a tenuous boundary between normal activity and
641 hyperactivity. Finally, we also observed that slightly increasing the initial $[Cl^-]_i$ of the neurons in
642 our model, comparable to the shift we observed following the reduction of $[A]_o$ with ChABC,
643 slightly promoted the spread of activity throughout our network (data not shown).

644 Our model demonstrates that the limited Cl^- extrusion capability of RT neurons, largely
645 dictated by expression of KCC2, has a considerable impact on the response of this nucleus to
646 excitatory drive. Specifically, the model predicts that RT neurons with a τ_{rec} of 32 seconds,
647 similar to what we measured experimentally, are more susceptible to an activity-dependent shift
648 towards GABA-mediated excitation than neurons with a faster τ_{rec}. This propensity for
649 undergoing a shift from inhibitory to excitatory GABAergic signaling allows weaker stimuli to
650 produce activation that spreads throughout the RT nucleus.

651

652 **Discussion**

653 We demonstrate that RT neurons maintain a low $[Cl^-]_i$ despite showing reduced
654 immunoreactivity for the Cl^- transporter KCC2. The limited KCC2 in RT neurons nonetheless
655 sustains a hyperpolarized E_{GABA}, but restricts Cl^- extrusion in response to prolonged GABAergic
656 signaling. RT neurons are therefore susceptible to an activity-dependent shift from inhibitory to
657 excitatory GABAergic signaling. Elevated impermeant anions surrounding RT neurons
658 contribute modestly to E_{GABA}. Overall, these findings support the importance of Cl^- transporters
659 and impermeant anions in regulating $[Cl^-]_i$ in the thalamus and enabling inhibitory GABAergic
660 signaling among RT neurons.

JNeurosci Accepted Manuscript

661 The RT nucleus is a gatekeeper of signaling between cortical and subcortical structures
662 (Jones, 1975; Pinault, 2004; McAlonan et al., 2008). Inhibition among RT neurons is
663 hypothesized to prevent seizures and suppress extraneous sensory input. Regarding the former
664 function, intra-RT inhibition is proposed to establish a seizure choke point that constrains the
665 widespread thalamic synchrony underlying generalized seizures (Sohal and Huguenard, 2003;
666 Paz and Huguenard, 2015; Makinson et al., 2017). Regarding the latter function, inhibitory RT
667 signaling is proposed to focus attention by filtering extraneous sensory stimuli (Crick, 1984;
668 McAlonan et al., 2008; Halassa et al., 2014; Wimmer et al., 2015; Wells et al., 2016).
669 Comprising this focusing mechanism produces sensory gating deficits. Indeed, hallucinations
670 and delusions associated with schizophrenia are hypothesized to result from RT neuron
671 dysfunction (Krause et al., 2003; Egerton et al., 2005; Ferrarelli and Tononi, 2011; Ahrens et al.,
672 2015). If seizure regulation and attention gating requires inhibition within the RT nucleus, then
673 we show that they do so under tenuous circumstances.
674
675 **GABAergic signaling inhibits RT neurons**
676 Utilizing electrophysiological and calcium imaging techniques, we find that RT neuron activity is,
677 in aggregate, inhibited by GABA. Our measured E_{GABA} for RT neurons (-62±3.0 mV) is
678 substantially more hyperpolarized than RT action potential threshold (~-47 mV; Dreyfus et al.,
679 2010; Muñoz and Fuentealba, 2012). As *in vivo* recordings reveal that RT neurons rest at -62
680 mV (Bazhenov et al., 1999), our results indicate that $GABA_A$ receptor activation clamps RT
681 neurons at their resting membrane potential. Indeed, our calcium imaging reveals that most RT
682 neurons respond to muscimol with minimal change in fluorescence (median ΔF/F = -2.8%,
683 interquartile range -7.1–4.8%, see **Fig. 2G**), suggesting that $GABA_A$ receptor activation does not
684 alter resting membrane potential. Even if RT neurons rest at -69 mV, as reported *in vitro* (Gentet
685 and Ulrich, 2003), then $GABA_A$ receptor activation would nonetheless promote shunting
686 inhibition (Edwards, 1990; Staley and Mody, 1992; Blaesse et al., 2009).

JNeurosci Accepted Manuscript

687 It remains possible that a subthreshold membrane depolarization resulting from $GABA_A$-
688 receptor activation evokes action potentials in RT neurons. Modest GABA-induced
689 depolarizations may recruit low voltage-activated, T-type Ca^{2+} channels that further depolarize
690 RT neurons towards firing threshold (Sun et al., 2012). If true, then a widespread increase in
691 muscimol-induced GCaMP fluorescence would likely result. However, muscimol only intensified
692 fluorescence in a few RT neurons, possibly reflecting cells initially resting at relatively
693 hyperpolarized membrane potentials with more available T-type channels (Perez-Reyes, 2003;
694 Dreyfus et al., 2010). Alternatively, brighter cells may have corresponded to the small
695 subpopulation of RT neurons with a more depolarized basal E_{GABA}, reflecting the heterogeneity
696 of distinct subpopulations known to exist within RT (Lee et al., 2007; Clemente-Perez et al.,
697 2017).

698

699 **KCC2 is an important regulator of $[Cl^-]_i$ in RT neurons**

700 Reduced KCC2 mRNA (Kanaka et al., 2001) and protein (Barthó et al., 2004; Sun et al., 2012)
701 in RT neurons of adult rodents predict that GABAergic signaling is excitatory. However,
702 anatomical experiments are unable to evaluate KCC2 function. Recording E_{GABA} with the
703 selective KCC antagonist VU0463271 reveals that even limited KCC2 in RT neurons contributes
704 to Cl^- homeostasis. While VU0463271 has minimal off-target interactions, it does inhibit α_{1B}
705 adrenergic receptors (Delpire et al., 2012; Sivakumaran et al., 2015). As adrenergic signaling
706 may alter KCC2 surface stability and transporter efficacy (Mahadevan and Woodin, 2016),
707 VU0463271 may alter $[Cl^-]_i$ via an indirect, albeit still KCC2-dependent mechanism. While
708 VU0463271 analogues antagonize other KCCs beyond KCC2 (Delpire and Weaver, 2016), the
709 thalamus appears to only express KCC2 (Rivera et al., 1999; Le Rouzic et al., 2006).

710 To validate VU0463271, we performed a subset of perforated patch recordings with a Cs-
711 based pipette solution. While this approach prevents anionic contamination of recorded
712 neurons, cations still diffuse through gramicidin pores and alter intracellular ionic concentrations

JNeurosci Accepted Manuscript

713 (Myers and Haydon, 1972). While K^+ and Cs^+ ions are both substrates for Cl^- transport by
714 KCC2, Cs^+ translocation occurs at a significantly slower rate, restricting Cl^- extrusion and
715 effectively inhibiting KCC2 (Williams and Payne, 2004). The occlusion of a VU0463271 effect by
716 Cs^+ indicates that both compounds impact E_{GABA} by blocking the action of KCC2. Cs-based
717 recording solutions have previously yielded noticeably higher measurements of $[Cl^-]_i$ in RT
718 neurons (Sun et al., 2012).
719
720 **$[A]_o$ only mildly impact $[Cl^-]_i$ regulation in RT neurons**
721 Our anatomical staining shows that CSPGs, a major source of $[A]_o$, are elevated in the RT
722 nucleus by the second postnatal week, consistent with past investigations (Vitellaro-Zuccarello
723 et al., 2001; Gáti et al., 2010). Regional and cell-type specific heterogeneity exists in CSPG
724 localization (Matthews et al., 2002), and WFA preferentially labels CSPGs surrounding
725 parvalbumin-positive interneurons (Gáti et al., 2010). Heightened WFA labeling surrounding RT
726 neurons matches the nearly homogenous population of parvalbumin-positive interneurons in
727 this nucleus. In contrast, the limited WFA labeling of VB neurons is attributed to a sparse
728 localization of CSPGs around the preterminal compartments of axons (Gáti et al., 2010).
729 While ChABC treatment increases $[Cl^-]_i$ in hippocampal neurons (Glykys et al., 2014a), we
730 observed no change in the basal E_{GABA} of RT or VB neurons following a two hour incubation in
731 ChABC. However, the E_{GABA} of ChABC treated RT neurons became more depolarized following
732 repeated measurement. This observation is consistent with the hypothesis that $[A]_o$ can define a
733 set point for E_{GABA}, but that other mechanisms likely provide the Cl^- flux required for the neuron
734 to equilibrate to this new level (Delpire and Staley, 2014). Our repeated measurements of E_{GABA}
735 involved repetitive $GABA_A$ receptor activation, which may have provided a sufficient Cl^- flux to
736 unmask the impact of ChABC treatment. Nevertheless, while Glykys et al. (2014a) found
737 ChABC treatment of hippocampal neurons produced a 16 mM increase in $[Cl^-]_i$, the greatest
738 change in E_{GABA} we observed in RT neurons was only equivalent to a 4 mM increase in $[Cl^-]_i$.

JNeurosci Accepted Manuscript

739 Utilizing a more intense ChABC treatment or a higher throughput technique to measure
740 changes in $[Cl^-]_i$, such as Clomeleon imaging (Dzhala et al., 2012; Wimmer et al., 2015), may
741 permit the unmasking of a greater contribution of $[A]_o$ to Cl^- homeostasis in thalamic neurons.
742

743 **Slow Cl^- extrusion enhances spreading activation among RT neurons**

744 While the steady-state E_{GABA} value measured in RT neurons supports inhibition, low KCC2
745 expression significantly slows Cl^- extrusion in RT neurons. Repeated $GABA_A$ receptor activation
746 produces rapid $[Cl^-]_i$ accumulation and an associated depolarizing GABAergic response (Staley
747 et al., 1995; Kuner and Augustine, 2000; Jedlicka et al., 2011). Having both weaker initial
748 GABAergic inhibition and a diminished capacity to recover from activity-dependent Cl^- influx, RT
749 neurons appear predisposed to shift towards excitatory GABAergic signaling when repeatedly
750 stimulated. Indeed, our computational model suggests that slow Cl^- extrusion leaves RT
751 neurons susceptible to undergoing an inhibitory-to-excitatory shift after receiving a train of
752 GABAergic inputs. Slower RT neuron Cl^- extrusion rates also correlate with a reduced threshold
753 to evoke excitatory signaling and accelerate the spread of excitatory GABAergic signaling
754 throughout the network. We hypothesize that this recapitulates the characteristic sudden onset
755 of absence seizures (Lüttjohann and Van Luijtelaar, 2015), occurring once the inhibitory choke
756 point formed by the RT nucleus is overwhelmed.

757 Years of anatomical evidence reveal the presence of GABAergic synapses onto RT
758 neurons (Ahlsén and Lindström, 1982; Yen et al., 1985; Ohara, 1988; Cox et al., 1996), and
759 electrophysiological studies suggest that RT neurons are functionally connected via GABAergic
760 synapses (Zhang and Jones, 2004; Deleuze and Huguenard, 2006; Makinson et al., 2017).
761 However, the existence of intra-RT connectivity remains debated (Landisman et al., 2002;
762 Cruikshank et al., 2010; Hou et al., 2016). Nevertheless, the substantia nigra pars reticulata
763 (Paré et al., 1990), globus pallidus (Nauta, 1979) and basal forebrain (Asanuma and Porter,
764 1990) also provide GABAergic input to RT neurons. These inputs will likewise inhibit RT neuron

JNeurosci Accepted Manuscript

765 activity, due to the low $[Cl^-]_i$ we have measured. Regardless of the source, $GABA_A$ receptor-
766 mediated signaling onto RT neurons modulates rhythmic thalamic oscillations. Both local
767 application of the $GABA_A$ antagonist bicuculline (Sanchez-Vives and McCormick, 1997) and
768 targeted knockdown of the $GABA_A$ subunit β_3 (Huntsman et al., 1999) selectively block
769 GABAergic signaling in the RT nucleus, without impacting other thalamic neurons. In both
770 cases, reducing $GABA_A$ receptor-mediated inputs to RT neurons promotes absence seizure-like
771 hypersynchronous oscillations.
772

773 **Conclusions**

774 In sum, the findings of this study demonstrate that GABAergic inhibition is tenuous within the
775 reticular thalamic (RT) nucleus. Weak chloride extrusion mechanisms render RT neurons
776 susceptible to an activity-dependent switch to GABAergic excitation. These findings have
777 important implications for RT's proposed role as a seizure choke point for generalized
778 epilepsies.
779

JNeurosci Accepted Manuscript

780 **References**

781

782 Ahlsén G, Lindström S (1982) Mutal inhibition between perigeniculate neurones. Brain Res
783 236:482–486.
784 Ahrens S, Jaramillo S, Yu K, Ghosh S, Hwang G-R, Paik R, Lai C, He M, Huang ZJ, Li B (2015)
785 ErbB4 regulation of a thalamic reticular nucleus circuit for sensory selection. Nat Neurosci
786 18:104–111.
787 Ajmo JM, Eakin AK, Hamel MG, Gottschall PE (2008) Discordant localization of WFA reactivity
788 and brevican/ADAMTS-derived fragment in rodent brain. BMC Neurosci 9:14.
789 Asanuma C, Porter LL (1990) Light and electron microscopic evidence for a GABAergic
790 projection from the caudal basal forebrain to the thalamic reticular nucleus in rats. J Comp
791 Neurol 302:159–172.
792 Bandtlow CE, Zimmermann DR (2000) Proteoglycans in the developing brain: new conceptual
793 insights for old proteins. Physiol Rev 80:1267–1290.
794 Barthó P, Payne JA, Freund TF, Acsády L (2004) Differential distribution of the KCl
795 cotransporter KCC2 in thalamic relay and reticular nuclei. Eur J Neurosci 20:965–975.
796 Bazhenov M, Timofeev I, Steriade M, Sejnowski TJ (1999) Self-sustained rhythmic activity in the
797 thalamic reticular nucleus mediated by depolarizing GABA A receptor potentials. Nat
798 Neurosci 2:168–174.
799 Blaesse P, Airaksinen MS, Rivera C, Kaila K (2009) Cation-chloride cotransporters and
800 neuronal function. Neuron 61:820–838.
801 Bormann J, Hamill OP, Sakmann B (1987) Mechanism of anion permeation through channels
802 gated by glycine and gamma-aminobutyric acid in mouse cultured spinal neurones. J
803 Physiol 385:243–286.
804 Cherubini E, Rovira C, Gaiarsa JL, Corradetti R, Ari Y Ben (1990) GABA mediated excitation in
805 immature rat CA3 hippocampal neurons. Int J Dev Neurosci 8:481–490.

JNeurosci Accepted Manuscript

806 Clemente-Perez A, Makinson SR, Higashikubo B, Brovarney S, Cho FS, Urry A, Holden SS,
807 Wimer M, Dávid C, Fenno LE, Acsády L, Deisseroth K, Paz JT (2017) Distinct Thalamic
808 Reticular Cell Types Differentially Modulate Normal and Pathological Cortical Rhythms.
809 Cell Rep 19:2130–2142.
810 Cox CL, Huguenard JR, Prince DA (1996) Heterogeneous axonal arborizations of rat thalamic
811 reticular neurons in the ventrobasal nucleus. J Comp Neurol 366:416–430.
812 Crick F (1984) Function of the thalamic reticular complex: the searchlight hypothesis. Proc Natl
813 Acad Sci 81:4586–4590.
814 Cruikshank SJ, Urabe H, Nurmikko A V, Connors BW (2010) Pathway-specific feedforward
815 circuits between thalamus and neocortex revealed by selective optical stimulation of axons.
816 Neuron 65:230–245.
817 Deleuze C, Huguenard JR (2006) Distinct electrical and chemical connectivity maps in the
818 thalamic reticular nucleus: potential roles in synchronization and sensation. J Neurosci
819 26:8633–8645.
820 DeLorey TM, Handforth A, Anagnostaras SG, Homanics GE, Minassian BA, Asatourian A,
821 Fanselow MS, Delgado-Escueta A, Ellison GD, Olsen RW (1998) Mice lacking the β3
822 subunit of the GABAA receptor have the epilepsy phenotype and many of the behavioral
823 characteristics of Angelman syndrome. J Neurosci 18:8505–8514.
824 Delpire E, Baranczak A, Waterson AG, Kim K, Kett N, Morrison RD, Daniels JS, Weaver CD,
825 Lindsley CW (2012) Further optimization of the K-Cl cotransporter KCC2 antagonist
826 ML077 : development of a highly selective and more potent in vitro probe. Bioorg Med
827 Chem Lett 22:4532–4535.
828 Delpire E, Staley KJ (2014) Novel determinants of the neuronal Cl- concentration. J Physiol
829 592:4099–4114.
830 Delpire E, Weaver CD (2016) Challenges of Finding Novel Drugs Targeting the K-Cl
831 Cotransporter. ACS Chem Neurosci 7:1624–1627.

JNeurosci Accepted Manuscript

832 Destexhe A, Bal T, Mccormick DA, Sejnowski TJ (1996) Ionic mechanisms underlying
833 synchronized oscillations and propagating waves in a model of ferret thalamic slices. J
834 Neurophysiol 76:2049–2070.
835 Donnan FG (1911) Theorie der membran gleichgewichte und membran potentiale bei
836 vorhandernsein von nicht dialysierenden elektrolyten. Zeitschrift für Elektrochimie und
837 Angewandlte Phys Chemie 17:572–581.
838 Doyon N, Prescott SA, De Koninck Y (2015) Mild KCC2 hypofunction causes inconspicuous
839 chloride dysregulation that degrades neural coding. Front Cell Neurosci 9:1–16.
840 Doyon N, Vinay L, Prescott SA, De Koninck Y (2016) Chloride Regulation: A Dynamic
841 Equilibrium Crucial for Synaptic Inhibition. Neuron 89:1157–1172.
842 Dreyfus FM, Tscherter A, Errington AC, Renger JJ, Shin H-S, Uebele VN, Crunelli V, Lambert
843 RC, Leresche N (2010) Selective T-Type Calcium Channel Block in Thalamic Neurons
844 Reveals Channel Redundancy and Physiological Impact of ITwindow. J Neurosci 30:99–
845 109.
846 Dzhala V, Valeeva G, Glykys J, Khazipov R, Staley K (2012) Traumatic Alterations in GABA
847 Signaling Disrupt Hippocampal Network Activity in the Developing Brain. J Neurosci
848 32:4017–4031.
849 Edwards DH (1990) Mechanisms of depolarizing inhibition at the crayfish giant motor synapse.
850 I. Electrophysiology. J Neurophysiol 64:541–550.
851 Egerton A, Reid L, McKerchar CE, Morris BJ, Pratt JA (2005) Impairment in perceptual
852 attentional set-shifting following PCP administration: A rodent model of set-shifting deficits
853 in schizophrenia. Psychopharmacology (Berl) 179:77–84.
854 Ferrarelli F, Tononi G (2011) The thalamic reticular nucleus and schizophrenia. Schizophr Bull
855 37:306–315.
856 Gáti G, Morawski M, Lendvai D, Jäger C, Négyessy L, Arendt T, Alpár A (2010) Distribution and
857 classification of aggrecan-based extracellular matrix in the thalamus of the rat. J Neurosci

JNeurosci Accepted Manuscript

858 Res 88:3257–3266.
859 Gentet LJ, Ulrich D (2003) Strong, reliable and precise synaptic connections between thalamic
860 relay cells and neurones of the nucleus reticularis in juvenile rats. J Physiol 546:801–811.
861 Glascock JJ, Osman EY, Coady TH, Rose FF, Shababi M, Lorson CL (2011) Delivery of
862 Therapeutic Agents Through Intracerebroventricular (ICV) and Intravenous (IV) Injection in
863 Mice. J Vis Exp:1–4.
864 Glykys J, Dzhala V, Egawa K, Balena T, Saponjian Y, Kuchibhotla K V, Bacskai BJ, Kahle KT,
865 Zeuthen T, Staley KJ (2014a) Local impermeant anions establish the neuronal chloride
866 concentration. Science 343:670–675.
867 Glykys J, Dzhala VI, Egawa K, Balena T, Saponjian Y, Kuchibhotla K V, Bacskai BJ, Kahle KT,
868 Zeuthen T, Staley KJ (2014b) Response to Comments on “Local impermeant anions
869 establish the neuronal chloride concentration.” Science 345:1130–d.
870 Halassa MM, Chen Z, Wimmer RD, Brunetti PM, Zhao S, Zikopoulos B, Wang F, Brown EN,
871 Wilson MA (2014) State-dependent architecture of thalamic reticular subnetworks. Cell
872 158:808–821.
873 Hines ML, Carnevale NT (1997) The NEURON simulation environment. Neural Comput 9:1179–
874 1209.
875 Homanics GE, DeLorey TM, Firestone LL, Quinlan JJ, Handforth A, Harrison NL, Krasowski
876 MD, Rick CEM, Korpi ER, Mäkelä R, Brilliant MH, Hagiwara N, Ferguson C, Snyder K,
877 Olsen RW (1997) Mice devoid of γ-aminobutyrate type A receptor β3 subunit have
878 epilepsy, cleft palate, and hypersensitive behavior. Proc Natl Acad Sci 94:4143–4148.
879 Horii-Hayashi N, Sasagawa T, Matsunaga W, Nishi M (2015) Development and Structural
880 Variety of the Chondroitin Sulfate Proteoglycans-Contained Extracellular Matrix in the
881 Mouse Brain. Neural Plast 2015.
882 Hou G, Smith AG, Zhang Z-W (2016) Lack of Intrinsic GABAergic Connections in the Thalamic
883 Reticular Nucleus of the Mouse. J Neurosci 36:7246–7252.

JNeurosci Accepted Manuscript

884 Huntsman MM, Huguenard JR (2006) Fast IPSCs in rat thalamic reticular nucleus require the
885 GABAA receptor beta1 subunit. J Physiol 572:459–475.
886 Huntsman MM, Porcello DM, Homanics GE, DeLorey TM, Huguenard JR (1999) Reciprocal
887 inhibitory connections and network synchrony in the mammalian thalamus. Science
888 283:541–543.
889 Jedlicka P, Deller T, Gutkin BS, Backus KH (2011) Activity-dependent intracellular chloride
890 accumulation and diffusion controls GABA(A) receptor-mediated synaptic transmission.
891 Hippocampus 21:885–898.
892 Jin X, Huguenard JR, Prince DA (2005) Impaired Cl- Extrusion in Layer V Pyramidal Neurons of
893 Chronically Injured Epileptogenic Neocortex. J Neurophysiol 93:2117–2126.
894 Jones EG (1975) Some aspects of the organization of the thalamic reticular complex. J Comp
895 Neurol 162:285–308.
896 Jones EG (2007) The Thalamus, 2nd ed. Cambridge: Cambridge University Press.
897 Kaila K, Price TJ, Payne JA, Puskarjov M, Voipio J (2014) Cation-chloride cotransporters in
898 neuronal development, plasticity and disease. Nat Rev Neurosci 15:637–654.
899 Kanaka C, Ohno K, Okabe A, Kuriyama K, Itoh T, Fukuda A, Sato K (2001) The differential
900 expression patterns of messenger RNAs encoding K-Cl cotransporters (KCC1,2) and Na-
901 K-2Cl cotransporter (NKCC1) in the rat nervous system. Neuroscience 104:933–946.
902 Krause M, Hoffmann WE, Hajós M (2003) Auditory sensory gating in hippocampus and reticular
903 thalamic neurons in anesthetized rats. Biol Psychiatry 53:244–253.
904 Kuner T, Augustine GJ (2000) A genetically encoded ratiometric indicator for chloride: capturing
905 chloride transients in cultured hippocampal neurons. Neuron 27:447–459.
906 Landisman CE, Long MA, Beierlein M, Deans MR, Paul DL, Connors BW (2002) Electrical
907 synapses in the thalamic reticular nucleus. J Neurosci 22:1002–1009.
908 Le Rouzic P, Ivanov TR, Stanley PJ, Baudoin FMH, Chan F, Pinteaux E, Brown PD, Luckman
909 SM (2006) KCC3 and KCC4 expression in rat adult forebrain. Brain Res 1110:39–45.

JNeurosci Accepted Manuscript

910 Lee S-H, Govindaiah G, Cox CL (2007) Heterogeneity of firing properties among rat thalamic
911 reticular nucleus neurons. J Physiol 582:195–208.
912 Luhmann HJ, Kirischuk S, Kilb W (2014) Comment on “Local impermeant anions establish the
913 neuronal chloride concentration.” Science 345:1130–c.
914 Lüttjohann A, Van Luijtelaar G (2015) Dynamics of networks during absence seizure’s on- and
915 offset in rodents and man. Front Physiol 6:1–17.
916 Mahadevan V, Woodin MA (2016) Regulation of neuronal chloride homeostasis by
917 neuromodulators. J Physiol 10:1–13.
918 Makinson CD, Tanaka BS, Sorokin JM, Wong JC, Christian CA, Goldin AL, Escayg A,
919 Huguenard JR (2017) Regulation of Thalamic and Cortical Network Synchrony by Scn8a.
920 Neuron 93:1165–1179.e6.
921 Matthews RT, Kelly GM, Zerillo CA, Gray G, Tiemeyer M, Hockfield S (2002) Aggrecan
922 glycoforms contribute to the molecular heterogeneity of perineuronal nets. J Neurosci
923 22:7536–7547.
924 McAlonan K, Cavanaugh J, Wurtz RH (2008) Guarding the gateway to cortex with attention in
925 visual thalamus. Nature 456:391–394.
926 McCormick DA, Prince DA (1986) Acetylcholine induces burst firing in thalamic reticular
927 neurones by activating a potassium conductance. Nature 319:402–405.
928 Muñoz F, Fuentealba P (2012) Dynamics of action potential initiation in the GABAergic thalamic
929 reticular nucleus in vivo. PLoS One 7:e30154.
930 Myers VB, Haydon DA (1972) Ion transfer across lipid membranes in the presence of gramicidin
931 A: II. The ion selectivity. Biochim Biophys Acta 274:313–322.
932 Nauta HJW (1979) Projections of the pallidal complex: An autoradiographic study in the cat.
933 Neuroscience 4:1853–1873.
934 Ohara PT (1988) Synaptic organization of the thalamic reticular nucleus. J Electron Microsc
935 Tech 10:283–292.

JNeurosci Accepted Manuscript

936 Paré D, Hazrati LN, Parent A, Steriade M (1990) Substantia nigra pars reticulata projects to the
937 reticular thalamic nucleus of the cat: a morphological and electrophysiological study. Brain
938 Res 535:139–146.
939 Payne JA, Stevenson TJ, Donaldson LF (1996) Molecular characterization of a putative K-Cl
940 cotransporter in rat brain: a neuronal-specific isoform. J Biol Chem 271:16245–16252.
941 Paz JT, Huguenard JR (2015) Microcircuits and their interactions in epilepsy: is the focus out of
942 focus? Nat Neurosci 18:351–359.
943 Perez-Reyes E (2003) Molecular Physiology of Low-Voltage-Activated T-type Calcium
944 Channels. Physiol Rev 83:117–161.
945 Pinault D (2004) The thalamic reticular nucleus: structure, function and concept. Brain Res
946 Brain Res Rev 46:1–31.
947 Pinault D, Smith Y, Deschênes M (1997) Dendrodendritic and axoaxonic synapses in the
948 thalamic reticular nucleus of the adult rat. J Neurosci 17:3215–3233.
949 Rivera C, Voipio J, Payne JA, Ruusuvuori E, Lahtinen H, Lamsa K, Pirvola U, Saarma M, Kaila
950 K (1999) The K+/Cl- co-transporter KCC2 renders GABA hyperpolarizing during neuronal
951 maturation. Nature 397:251–255.
952 Rohrbough J, Spitzer NC (1996) Regulation of intracellular Cl- levels by Na(+)-dependent Cl-
953 cotransport distinguishes depolarizing from hyperpolarizing GABAA receptor-mediated
954 responses in spinal neurons. J Neurosci 16:82–91.
955 Sanchez-Vives M V, McCormick DA (1997) Functional properties of perigeniculate inhibition of
956 dorsal lateral geniculate nucleus thalamocortical neurons in vitro. J Neurosci 17:8880–
957 8893.
958 Sivakumaran S, Cardarelli RA, Maguire J, Kelley MR, Silayeva L, Morrow DH, Mukherjee J,
959 Moore YE, Mather RJ, Duggan ME, Brandon NJ, Dunlop J, Zicha S, Moss SJ, Deeb TZ
960 (2015) Selective Inhibition of KCC2 Leads to Hyperexcitability and Epileptiform Discharges
961 in Hippocampal Slices and In Vivo. J Neurosci 35:8291–8296.

JNeurosci Accepted Manuscript

962 Sohal VS, Huguenard JR (2003) Inhibitory interconnections control burst pattern and emergent
963 network synchrony in reticular thalamus. J Neurosci 23:8978–8988.
964 Staley K, Smith R (2001) A new form of feedback at the GABA(A) receptor. Nat Neurosci
965 4:674–676.
966 Staley KJ, Mody I (1992) Shunting of excitatory input to dentate gyrus granule cells by a
967 depolarizing GABAA receptor-mediated postsynaptic conductance. J Neurophysiol 68:197–
968 212.
969 Staley KJ, Soldo BL, Proctor WR (1995) Ionic Mechanisms of Neuronal Excitation by Inhibitory
970 GABAA Receptors. Science 269:977–981.
971 Sun Y-G, Wu C-S, Renger JJ, Uebele VN, Lu H-C, Beierlein M (2012) GABAergic synaptic
972 transmission triggers action potentials in thalamic reticular nucleus neurons. J Neurosci
973 32:7782–7790.
974 Ting JT, Daigle TL, Chen Q, Feng G (2014) Acute brain slice methods for adult and aging
975 animals: application of targeted patch clamp analysis and optogenetics. In: Patch-Clamp
976 Methods and Protocols, 2nd ed. (Martina M, Taverna S, eds), pp 221–242 Methods in
977 Molecular Biology. New York, NY: Springer New York.
978 Ulrich D, Huguenard JR (1997) Nucleus-specific chloride homeostasis in rat thalamus. J
979 Neurosci 17:2348–2354.
980 Vitellaro-Zuccarello L, Meroni A, Amadeo A, De Biasi S (2001) Chondroitin sulfate
981 proteoglycans in the rat thalamus: Expression during postnatal development and
982 correlation with calcium-binding proteins in adults. Cell Tissue Res 306:15–26.
983 Voipio J, Boron WF, Jones SW, Hopfer U, Payne JA, Kaila K (2014) Comment on “Local
984 impermeant anions establish the neuronal chloride concentration.” Science 345:1130–b.
985 Wells MF, Wimmer RD, Schmitt LI, Feng G, Halassa MM (2016) Thalamic reticular impairment
986 underlies attention deficit in Ptchd1(Y/-) mice. Nature 532:58–63.
987 Williams JR, Payne JA (2004) Cation transport by the neuronal K(+)-Cl(-) cotransporter KCC2:

JNeurosci Accepted Manuscript

988 thermodynamics and kinetics of alternate transport modes. Am J Physiol Cell Physiol
989 287:C919–C931.
990 Wimmer RD, Schmitt LI, Davidson TJ, Nakajima M, Deisseroth K, Halassa MM (2015) Thalamic
991 control of sensory selection in divided attention. Nature 526:705–709.
992 Wobbrock JO, Findlater L, Gergle D, Higgins JJ (2011) The aligned rank transform for
993 nonparametric factorial analyses using only ANOVA procedures. In: Proceedings of the
994 ACM Conference on Human Factors in Computing Systems (CHI '11). Vancouver, British
995 Columbia (May 7-12, 2011), pp 143–146. New York: ACM.
996 Wong CGT, Bottiglieri T, Snead OC (2003) GABA, gamma-hydroxybutyric acid, and
997 neurological disease. Ann Neurol 54:S3–S12.
998 Yamagata T, Saito H, Habuchi O, Suzuki S (1968) Purification and Properties and
999 Chondrosulfatases " of Bacterial Chondroitinases. J Biol Chem 243:1523–1535.
1000 Yen CT, Conley M, Hendry SHC, Jones EG (1985) The morphology of physiologically identified
1001 GABAergic neurons in the somatic sensory part of the thalamic reticular nucleus in the cat.
1002 J Neurosci 5:2254–2268.
1003 Zhang L, Jones EG (2004) Corticothalamic inhibition in the thalamic reticular nucleus. J
1004 Neurophysiol 91:759–766.
1005
1006

JNeurosci Accepted Manuscript

1007 **Figure Legends**

1008

1009 **Figure 1. KCC2 expression is low in RT neurons throughout development.** ***A***,
1010 Immunofluorescence of parvalbumin (green) and KCC2 (red) in horizontal sections of rat
1011 thalamus at different developmental time points. All images are oriented with the anterior (A)
1012 aspect of the thalamus towards the top, the lateral (L) aspect towards the right and the internal
1013 capsule (IC) towards the upper right corner of the image. Dotted lines indicate the boundaries of
1014 the RT nucleus in the enlarged images. ***B***, KCC2 immunofluorescence increased across the
1015 ages we tested. KCC2 labeling was consistently lower in the RT nucleus, relative to VB, across
1016 the ages tested. A similar pattern of KCC2 labeling was observed in mice. ***C***, Schematic of
1017 methodology for measuring regional variability in KCC2 intensity across segments of the RT
1018 nucleus. Intensity of KCC2 labeling was measured in an ROI, subdivided into 10 segments, that
1019 extended from the anterior to the lateral extent of the RT nucleus (see ***A***, lower left) and values
1020 were normalized to the mean intensity across this entire span. ***D***, KCC2 labeling was consistent
1021 throughout the span of the RT nucleus at P10, but showed significant regional variability in P40
1022 rats and mice. $^*p<0.05$; $^{**}p<0.01$; $^{***}p<0.001$.

1023

1024 **Figure 2. RT neurons maintain a relatively low $[Cl^-]_i$.** Gramicidin perforated patch recordings
1025 of muscimol-induced (100 μM, 10 ms) currents from RT (***A***) and VB (***B***) neurons at various
1026 command potentials. The leak current has been subtracted from the representative traces. The
1027 intersection of the pre-stimulation leak current and the muscimol-induced current was used to
1028 determine the $GABA_A$ receptor-mediated equilibrium potential (E_{GABA}, indicated by red arrow). ***C***,
1029 The E_{GABA} of RT neurons was more depolarized than in VB neurons, yet remained at levels that
1030 likely support inhibitory GABAergic signaling. ***D***, GCaMP6s was expressed in RT neurons for
1031 calcium imaging experiments and a local perfusion system provided timed delivery of muscimol
1032 (5 μM) or elevated KCl (+10 mM) to the imaged RT nucleus. ***E***, Two minute application of

JNeurosci Accepted Manuscript

1033 muscimol mostly decreased the fluorescence of RT neurons. ROIs drawn around GCaMP6s
1034 expressing RT neurons are colored according to their peak change in fluorescence.
1035 Representative examples of neurons displaying the minimum (***E1***), median (***E2***) and maximum
1036 (***E3***) fluorescence change in a particular brain slice following muscimol application. ***F***, Two
1037 minutes of elevated KCl produced a nearly uniform increase in the fluorescence of RT neurons.
1038 Examples of the minimum (***F1***), median (***F2***) and maximum (***F3***) fluorescence changes evoked
1039 by elevated KCl application. ***G***, Histograms comparing induced responses in all cells imaged,
1040 across multiple animals, shows that the median response (dotted line) to muscimol was a slight
1041 decrease in fluorescence. In contrast, mild depolarization with elevated KCl produced a robust
1042 increase in fluorescence. Bin size: 5ΔF/F(%). ***p<0.001.
1043

1044 **Figure 3. CSPGs are elevated around RT neurons**. ***A***, Immunofluorescence of parvalbumin
1045 (green) and labeling of CSPGs with WFA (red) in horizontal sections of rat thalamus at different
1046 developmental time points. All images are oriented with the anterior (A) aspect of the thalamus
1047 towards the top, the lateral (L) aspect towards the right. Dotted lines indicate the boundaries of
1048 the RT nucleus in the enlarged images. ***B***, WFA staining increased across the ages we tested
1049 and was consistently elevated in the RT nucleus, relative to VB. ***C***, Intensity of WFA labeling
1050 was measured in an ROI, subdivided into 10 segments, that extended from the anterior to the
1051 lateral extent of the RT nucleus (see ***A***, lower left, **Fig. 1C**) and values were normalized to the
1052 mean intensity across this entire span. WFA labeling showed slight regional variability in both
1053 P10 and P40 rats. A similar pattern of WFA labeling was observed in mice. **p<0.01; ***p<0.001
1054

1055 **Figure 4. CSPGs mildly contribute to setting E_{GABA} in RT neurons**. Gramicidin perforated
1056 patch recordings of muscimol-induced (100 μM, 10 ms) currents from RT (***A***) and VB (***B***)
1057 neurons at various command potentials, following a 2 hour incubation in ChABC (0.4 U/ml,
1058 37°C). The leak current has been subtracted from the representative traces. E_{GABA} was

JNeurosci Accepted Manuscript

1059 determined from the intersection of the pre-stimulation leak current and the muscimol-induced
1060 current (red arrow). ***C***, ChABC did not alter the initial measurement of E_{GABA} in either RT or VB
1061 neurons, relative to control neurons incubated in the absence of ChABC. ***D***, When E_{GABA}
1062 measurements were repeated every 2.5 minutes, ChABC treatment produced a small
1063 depolarizing shift in E_{GABA} in RT neurons. ***E***, No time dependent shift in E_{GABA} occurred in
1064 ChABC-treated VB neurons. ***F***, Immunofluorescence of parvalbumin (green) and labeling of
1065 CSPGs with WFA (red) of control and ChABC-treated thalamic slices (300µm) indicates that
1066 ChABC (0.4 U/ml, 37°C) effectively reduces CSPGs surrounding RT neurons. ***G***, WFA labeling
1067 in the RT nucleus of ChABC-treated slices was reduced relative to control slices. ***H***, WFA
1068 labeling in RT was first normalized to VB levels, thereby revealing a clear effect of ChABC
1069 treatment. **$p<0.01$; ***$p<0.001$.
1070
1071 **Figure 5. KCC2 regulates E_{GABA} in RT**. Gramicidin perforated patch recordings of muscimol-
1072 induced (100 µM, 10 ms) currents from RT (***A***) and VB (***B***) neurons at various command
1073 potentials were altered by application of the specific KCC2 antagonist VU0463271 (10 µM).
1074 ***A1,B1*** A depolarizing shift in E_{GABA} occurring between baseline (black traces) and after 10
1075 minutes of VU0463271 application (gray traces) was reflected in a shifted intersection between
1076 the pre-stimulation leak current and the muscimol-induced current. The leak current has been
1077 subtracted from the representative traces. This depolarizing shift was apparent when the time
1078 course of the shift in E_{GABA} was measured (***A2,B2***), and when baseline and 10 minutes post
1079 VU0463271 E_{GABA} values where compared (***A3,B3***). ***C***, Calcium imaging of GCaMP6s
1080 expressing RT neurons, preincubated in VU0463271 (10 µM) for 5 minutes, display a mixed
1081 response to a two minute application of muscimol (5 µM) through a local perfusion system. ROIs
1082 drawn around GCaMP6s expressing RT neurons are colored according to their peak change in
1083 fluorescence. Examples of the minimum (***C1***), median (***C2***) and maximum (***C3***) fluorescence
1084 change in a particular brain slice following muscimol application. ***D***, Two minutes of elevated

JNeurosci Accepted Manuscript

1085 KCl still produced a nearly uniform increase in the fluorescence of RT neurons preincubated in
1086 VU0463271. Examples of the minimum (***D1***), median (***D2***) and maximum (***D3***) fluorescence
1087 changes evoked by elevated KCl application. ***E***, Histograms comparing induced responses in all
1088 cells imaged, across multiple animals. Muscimol produced a slight increase in the median
1089 response. In contrast, mild depolarization with elevated KCl produced a robust increase in
1090 fluorescence. Bin size: 5ΔF/F(%). ***F***, In a comparison of the median GCaMP6s response, per
1091 brain slice, pretreatment with VU0463271 produced a greater increase in fluorescence, across
1092 the stimuli tested. ***G***, Gramicidin perforated patch recordings of muscimol-induced (100 μM, 10
1093 ms) currents in RT neurons pretreated with ChABC (0.4 U/ml, 2 hours at 37°C) displayed a
1094 greater depolarizing shift in E_{GABA} following VU0463271 application (10 μM) than did control
1095 treated neurons. *p<0.05; **p<0.01; ***p<0.001.
1096

1097 **Figure 6. Cs alters $[Cl^-]_i$ homeostasis in RT neurons**. Gramicidin perforated patch recordings
1098 of muscimol-induced currents from RT (***A***) and VB (***B***) neurons at various command potentials,
1099 using a CsCl-based internal solution. The leak current has been subtracted from the
1100 representative traces. ***A1***, Baseline E_{GABA} was more depolarized than in prior recordings with a
1101 KCl-based internal solution. Representative recording and current-voltage plot are shown. ***A2***,
1102 Time series revealing that CsCl-based solutions mitigated the effect of VU0463271 application
1103 in E_{GABA}, relative to KCl-based recordings (**Fig. 5**). ***A3***, Average change in E_{GABA} before and
1104 after 10 minutes of VU0463271 application. ***B1-3***. Similar measures examined in VB neurons,
1105 as described in A1-3. VU0463271 application still shifted E_{GABA} in VB neurons, although the
1106 responses were blunted. *p<0.05; **p<0.01.
1107

1108 **Figure 7. Recovery from Cl^- loading is limited in RT neurons**. ***A***, Schematics of protocol for
1109 Cl^- loading experiments. Neurons were voltage clamped at -30 mV for 500 ms and then ramped
1110 from -100 to -10 mV over a duration of 500 ms (left). This protocol lasted one second and was

JNeurosci Accepted Manuscript

1111 repeated 100 times per cell (right). After 10 sec of baseline recording, Cl^- was loaded by
1112 applying 10 puffs of muscimol (20 ms, 100 μM), once every three seconds, while the neuron
1113 was held at -30 mV. ***B***, Gramicidin perforated patch recordings of RT and VB neurons during
1114 measurement of Cl^- loading and recovery. E_{GABA} was measured by finding the point in the
1115 voltage ramp where the membrane current responses from before (a) and during (b) muscimol
1116 application intersected (marked by dotted line). Cl^- recovery was measured by tracking the
1117 change in E_{GABA} following the last application of muscimol (a vs. c). Single-exponential functions
1118 were fit to the shifting E_{GABA} occurring in RT (***C***) and VB (***D***) neurons to determine time
1119 constants for Cl^- loading and recovery. ***E***, The change in E_{GABA} (ΔE_{GABA}) was measured between
1120 the start of Cl^- loading and the final reading during Cl^- recovery (see inset in ***C***). This
1121 measurement indicates that chloride loading occurs rapidly in RT neurons. ***F***, The basal Cl^-
1122 recovery rate (τ_{rec}) was slower in RT than in VB neurons. The τ_{rec} in RT neurons was unaffected
1123 by a 10 minute application of VU0463271 (***G***, 10 μM), but became slower in VB neurons (***H***). ***I***,
1124 A two hour incubation in ChABC (0.4 U/ml, 37°C) did not alter the τ_{rec} of either RT or VB
1125 neurons. *p<0.05; **p<0.01; ***p<0.001.
1126

1127 **Figure 8. Computational modeling of $[Cl^-]_i$ dynamics in a network of RT neurons**. ***A***,
1128 Network composed of a linear array of 100 RT neurons, each projecting GABAergic synapses to
1129 the eight nearest neurons. Current injections to Cells 46, 51 and 56 simulated excitatory inputs
1130 to this network. ***B***, Graphical representation of evolving $[Cl^-]_i$ within all model RT neurons over
1131 time. Action potential activity generated by individual model RT neurons is overlaid. White
1132 vertical lines indicate action potentials in neurons directly receiving current injection, while black
1133 vertical lines indicate synaptically-evoked action potentials. In a network wherein Cells 46, 51
1134 and 56 received 30 Hz stimulation and all cells were characterized by a Cl^- recovery rate (τ_{rec}) of
1135 32 sec, $[Cl^-]_i$ initially increased only in the neurons receiving direct GABAergic projections from

JNeurosci Accepted Manuscript

1136 the stimulated cells. Over time, however, activity propagated throughout the entire network. ***C***,
1137 Example V_m (red) and $[Cl^-]_i$ (blue) traces from Cells 51, 53 and 80 from ***B***. Cell 51 received
1138 direct, current stimulation. Cell 53 received monosynaptic input from a stimulated cell. Cell 80
1139 was more distant from the site of stimulation. Expanded insets show the shifts in V_m and $[Cl^-]_I$ at
1140 various time points during the propagation of activity within the RT network (***C1-3***). When $[Cl^-]_i$
1141 became sufficiently elevated for GABAergic signaling to evoke action potentials in these
1142 neurons (***C2***), the rise in $[Cl^-]_i$ began to spread throughout the network, along with an increase in
1143 the number of cells firing action potentials (***C3***). ***D***, Higher frequency stimulation increased the
1144 number of activated neurons (arrows indicate the inflection point where activation first occurs)
1145 and (***E***) decreased the time required to first evoke action potentials (Cell 53, solid lines; Cell 80,
1146 dashed lines). ***F***, Both slower τ_{rec} and more frequent stimulation were correlated with an
1147 increased likelihood of activity spreading within the RT nucleus.

JNeurosci Accepted Manuscript

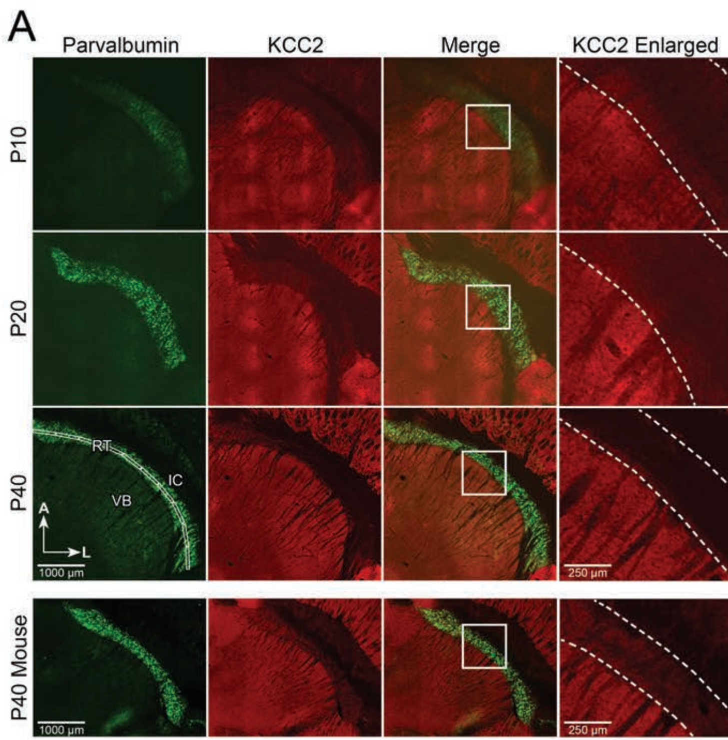

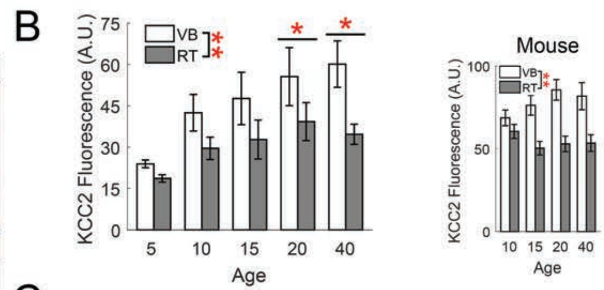

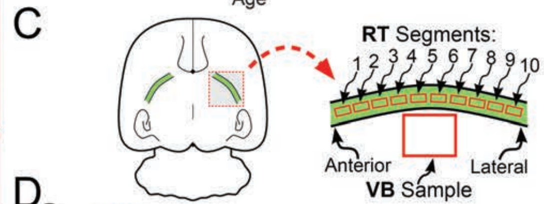

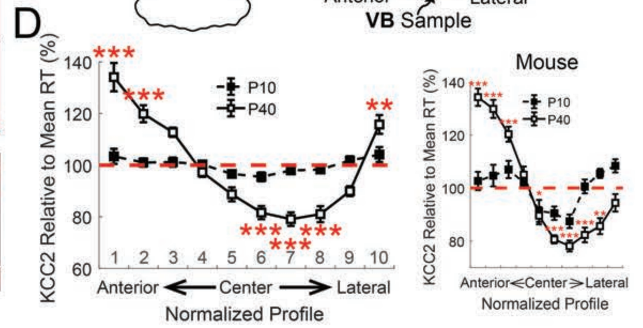

JNeurosci Accepted Manuscript

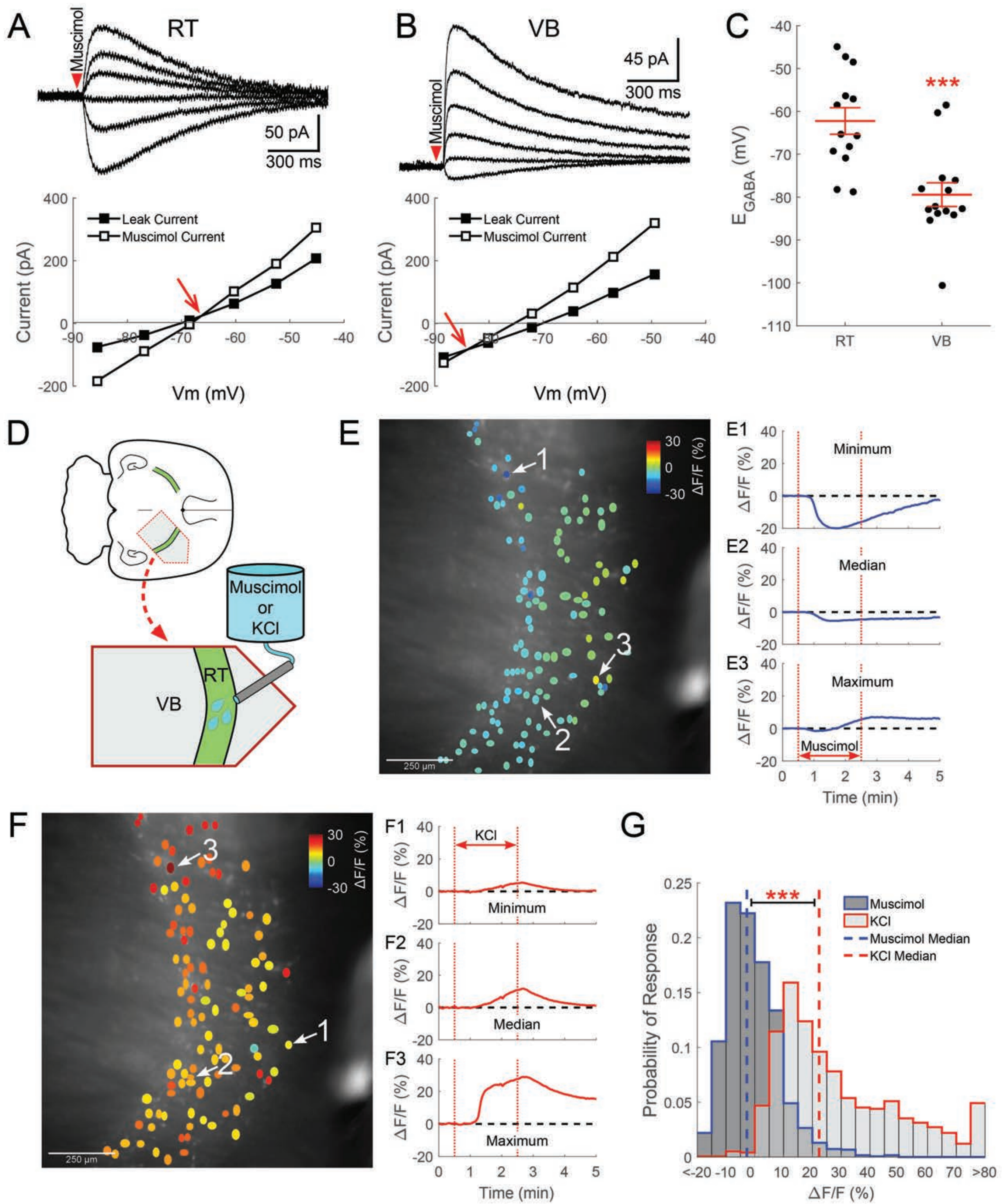

JNeurosci Accepted Manuscript

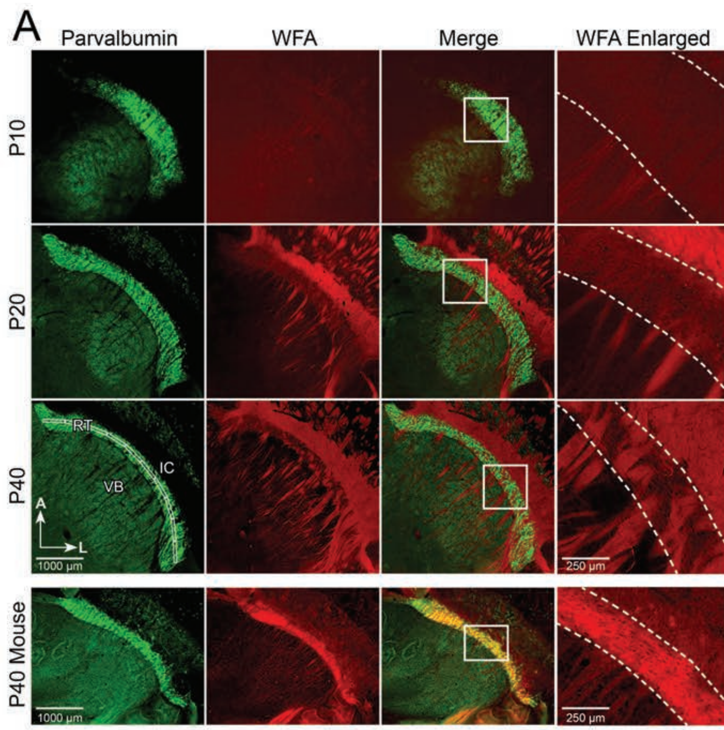

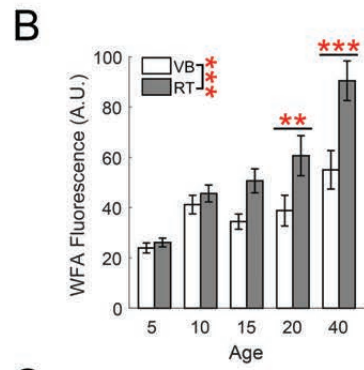

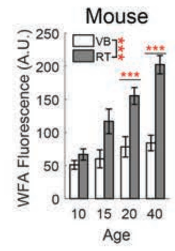

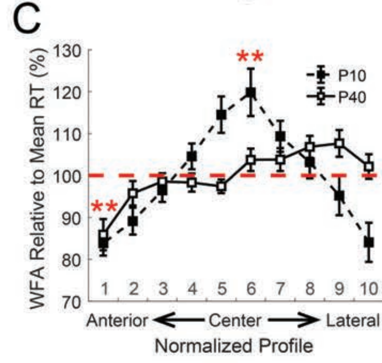

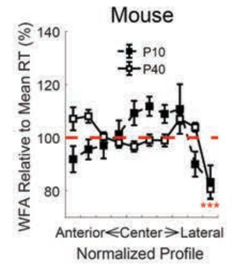

JNeurosci Accepted Manuscript

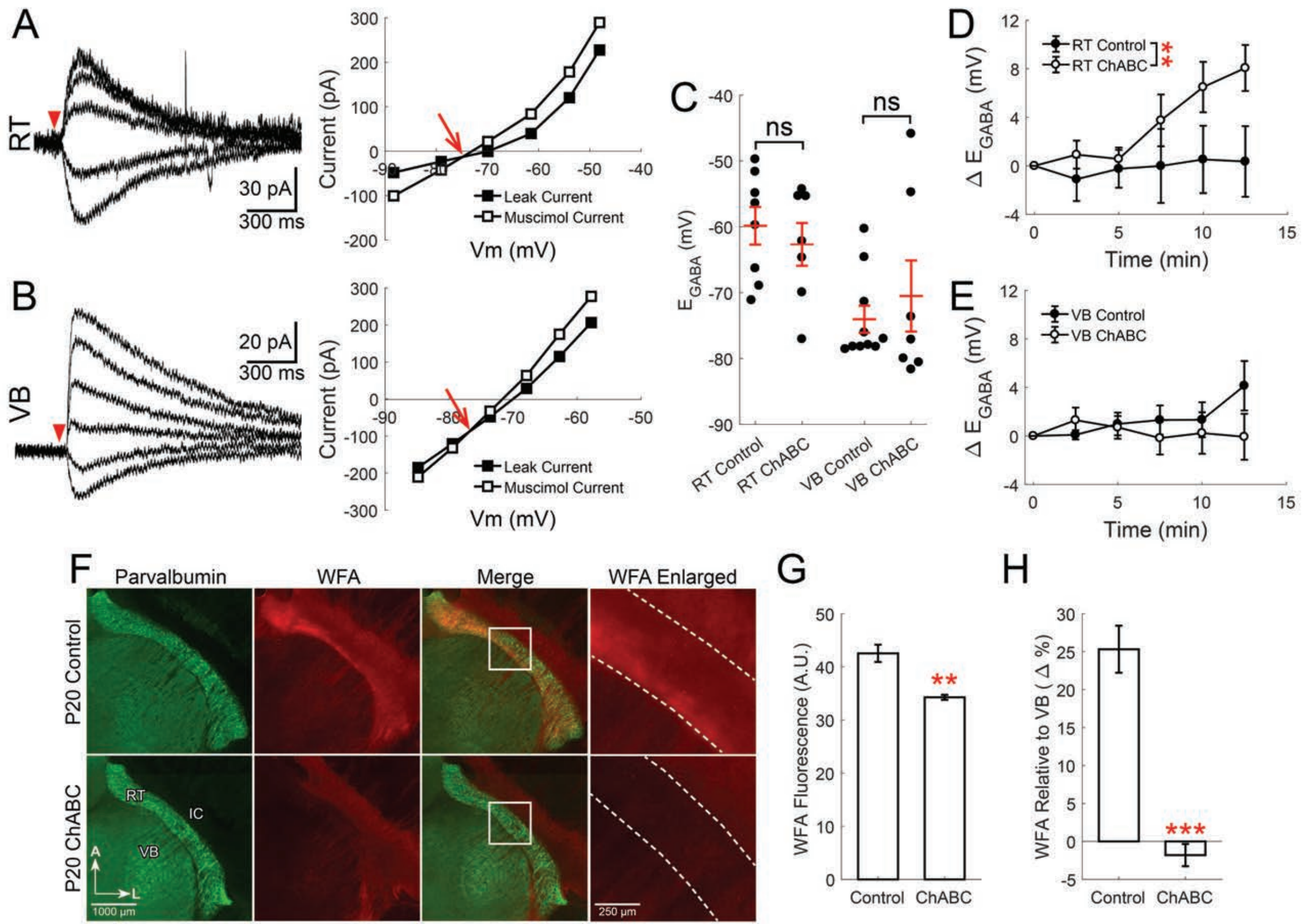

JNeurosci Accepted Manuscript

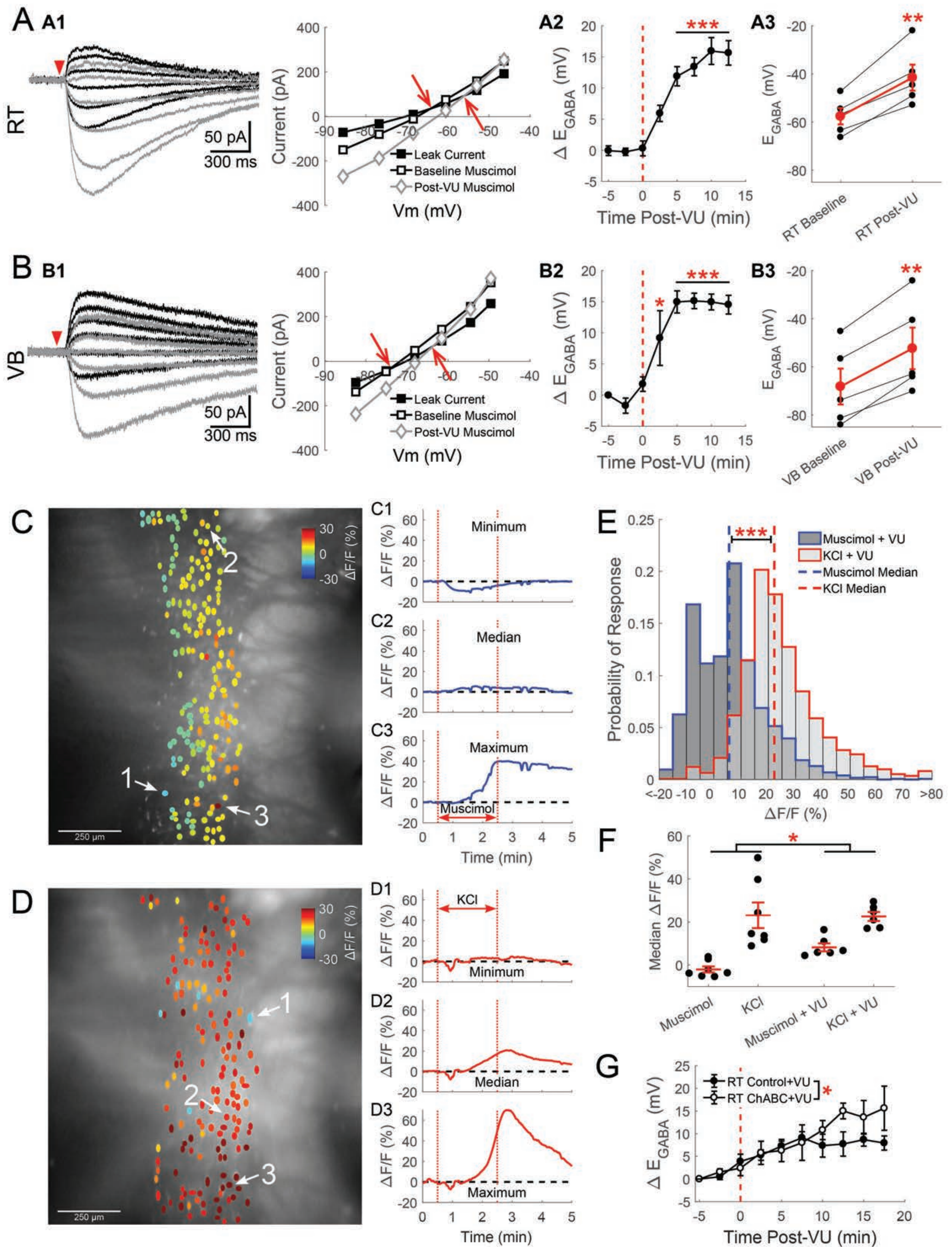

JNeurosci Accepted Manuscript

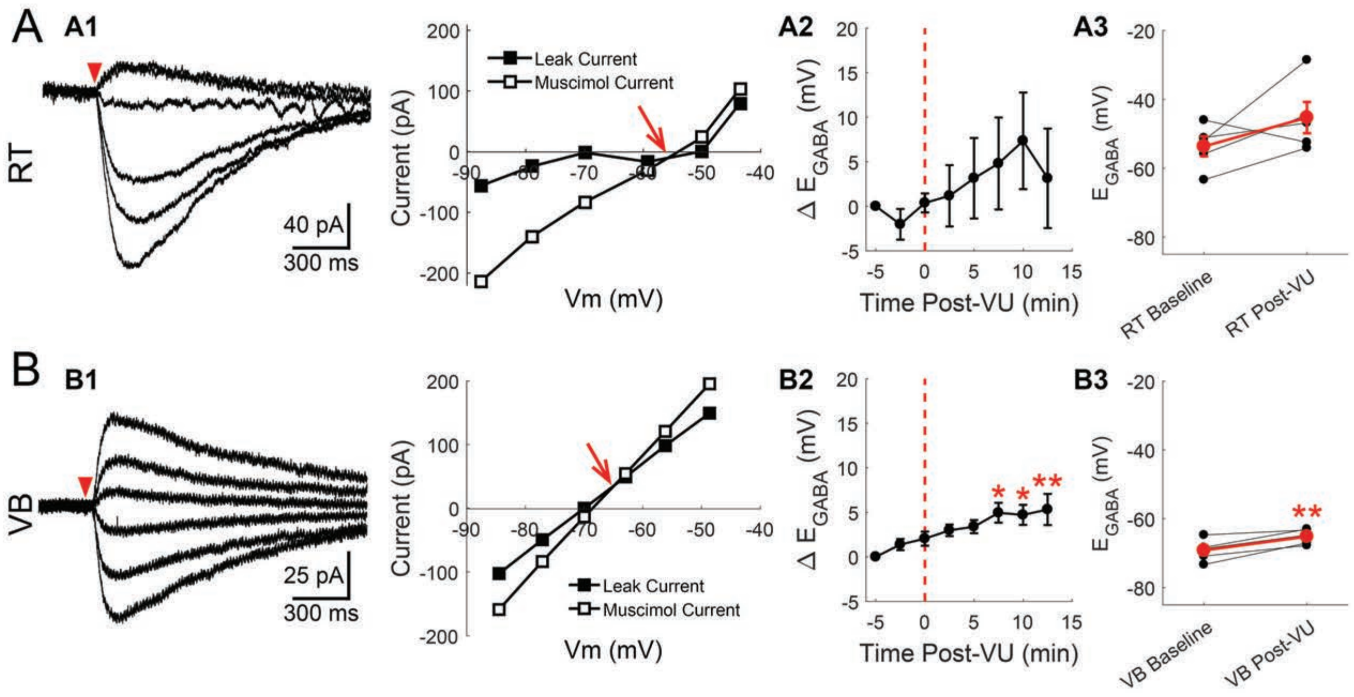

JNeurosci Accepted Manuscript

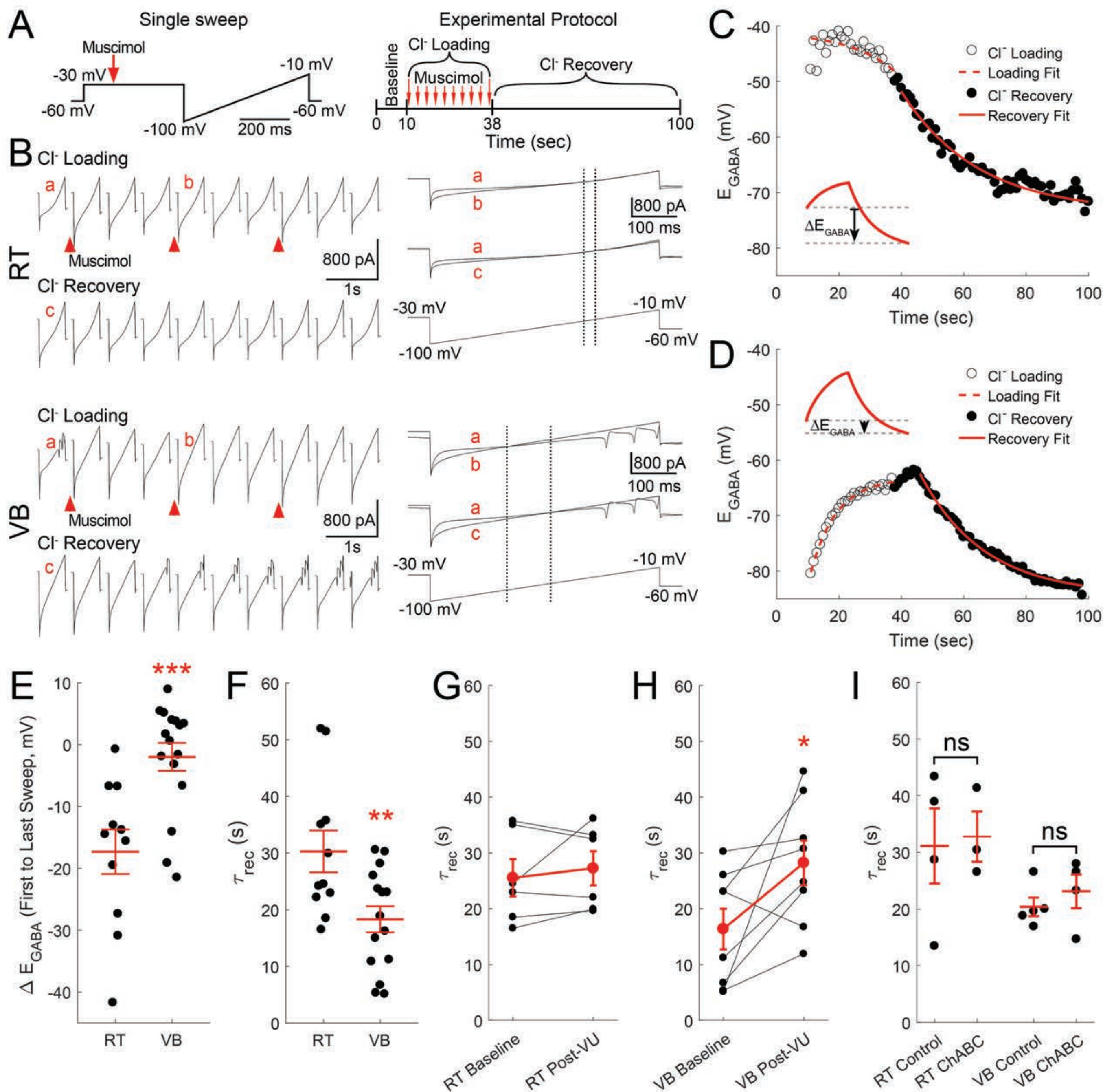

JNeurosci Accepted Manuscript